6

c.2

NACA

RESEARCH MEMORANDUM

FLUTTER INVESTIGATION IN THE HIGH SUBSONIC AND TRANSONIC SPEED RANGE ON CANTILEVER DELTA-WING PLAN FORMS WITH LEADING-EDGE SWEEPBACK OF 60°, 53° 8', AND 45°

By William T. Lauten, Jr., and Marvin F. Burgess

Langley Aeronautical Laboratory
Langley Field, Va.

NATIONAL ADVISORY COMMITTEE
FOR AERONAUTICS

WASHINGTON

January 31, 1957

NACA RM L56K26

NATIONAL ADVISORY COMMITTEE FOR AERONAUTICS

RESEARCH MEMORANDUM

FLUTTER INVESTIGATION IN THE HIGH SUBSONIC AND TRANSONIC SPEED RANGE ON CANTILEVER DELTA-WING PLAN FORMS WITH LEADING-EDGE SWEEPBACK OF 60°, 53° 8', AND 45°

By William T. Lauten, Jr., and Marvin F. Burgess

SUMMARY

Results of flutter tests on three cantilever delta-wing plan forms (leading-edge sweepback of 60°, 53° 8', and 45°) at Mach numbers from 0.4 to 1.0 are presented herein. One result was that the ratio of the second bending frequency to the torsion frequency had a marked effect on the flutter susceptibility of the wing. There was also a marked compressibility effect which led to the conclusion that over the range investigated the transonic Mach number range was the region where flutter was most likely to occur for these plan forms when flown at either constant dynamic pressure or constant altitude.

Structural influence coefficients were obtained on a few wings of each plan form and these coefficients and calculated mode shapes and frequencies derived therefrom are presented.

A reference flutter speed is calculated for several of the tests for the purposes of comparison and in order to make the data more general. This reference flutter speed is based on a theory which includes the effect of mode shape (for simplicity, only the first bending and first torsion modes were utilized), a correction for sweep, and the use of two-dimensional flutter derivatives. The addition of a third mode (second bending) to the calculations for one 60° wing makes only a small difference in the final answer but in another case the addition of the second bending mode increases by 50 percent the result obtained when only two modes are used.

A comparison is also made with an empirically derived criterion which involves test density and geometric, stiffness, and mass characteristics of the plan form. The predicted speed is generally somewhat unconservative and apparently the criterion is not applicable at low test densities or to flutter involving the higher modes.

INTRODUCTION

In view of the current interest of designers in the delta-wing plan form and since few flutter data are available for this plan form in the transonic Mach number range, it was felt that a limited series of tests on delta wings in this range would be desirable.

Previous flutter work in the transonic range has dealt primarily with more conventional plan forms ranging from unswept untapered wings of high aspect ratio (ref. 1) to 60° swept wings with taper ratio of 0.2 and aspect ratio as low as 3 (refs. 2 and 3). Transonic tests of cropped delta wings are reported in reference 4 and of two 64° delta wings in reference 5. Subsonic tests are reported in reference 6.

This paper reports flutter data obtained in the Langley 8-foot transonic pressure tunnel on delta wings with leading-edge sweepback of 60°, 53° 8', and 45°, with emphasis on the 60° plan form, at Mach numbers from 0.4 to 1.0. Wings of two frequency spectra were tested - one spectrum with the second natural bending frequency lower than first natural torsion frequency and the other with the second bending higher than torsion. Structural influence coefficients, and mode shapes and frequencies derived from these coefficients, are presented. In order to make the flutter information presented more general, the two-dimensional incompressible-flow flutter theory of reference 7 and, as an alternate method, the empirically derived criterion of reference 4 are applied as a means of normalizing the results obtained.

SYMBOLS

A	aspect ratio
a	nondimensional wing-reference-axis position measured in streamwise direction from midchord, positive for axis behind midchord, $\frac{2x_o}{100} - 1$
$a + x_\alpha$	nondimensional wing center of gravity measured in streamwise direction from midchord, positive for center of gravity behind midchord, $\frac{2x_1}{100} - 1$
b	semichord of test wing measured in the stream direction, ft

[redacted]

H	calculated mode shape, $\frac{\text{Vertical displacement of any section}}{\text{Vertical displacement of section with maximum displacement}}$
f	frequency, cps
I_α	polar mass moment of inertia about elastic axis per unit length, ft-lb-sec^2/ft
μ	mass ratio, $m/\pi\rho b^2$
Λ	sweepback of leading edge, deg
l	length perpendicular to free stream, in.
M	Mach number
m	mass of wing per unit length along semispan, slugs/ft
ω	frequency, radians/sec
ρ	air density, slugs/cu ft
q	dynamic pressure, lb/sq ft
r_α^2	square of nondimensional radius of gyration about elastic axis, I_α/mb^2
s	exposed semispan, measured from free-stream root of model, in.
V	velocity, fps
V_c	velocity of sound, fps
V_R	flutter velocity derived from calculations based on two-dimensional incompressible-flow theory of reference 7, fps
V_2	flutter velocity derived from criterion given in reference 4, fps
x_o	distance of reference axis of wing section behind leading edge measured in stream direction, percent chord
x_1	distance of center of gravity of wing section behind leading edge measured in stream direction, percent chord

Subscripts:

e	experimental values obtained at start of sustained flutter
f	flutter frequency
h_1	first bending
h_2	second bending
α	first torsion
R	calculated values based on two-dimensional incompressible-flow theory of reference 7
r	values taken at free-stream root section
s	values based on standard atmosphere

MODELS AND TEST PROCEDURE

Construction of Test Wings

In order to obtain a variation of frequency spectrum, with primary attention directed to the ratio of the second natural bending frequency to the first natural torsional frequency, two basic types of construction were used.

The first type of wing was built to have a frequency spectrum of first bending, torsion, and second bending in that order. These wings were built of spruce and aluminum alloy or spruce and balsa laminated in such a manner that the flexural and torsional rigidity of the spanwise sections were approximately proportional to the fourth power of the streamwise chord and the mass of each spanwise section was approximately proportional to the square of the streamwise chord. Figure 1 shows a cross section of two 60° delta wings, designated type A and type B, which had this type of construction. With the construction as shown, these wings could not be fluttered in the q-range of the tunnel. Consequently, streamwise slots 1 inch apart starting 1 inch from the root were cut into the upper and lower surface. For type A the slot depth was about two-thirds the thickness of the balsa and for type B the slots went completely through the balsa. The stiffness and vibration data presented later are for the weakened wings. Figure 1 also shows a cross section of the 45° and 53° 8' delta wings (type D) which were made of spruce and aluminum alloy.

The second type of wing was built to have a frequency spectrum of first bending, second bending, and torsion in that order. These wings were built of balsa, aluminum foil, and aluminum-alloy sheet. A core was constructed of balsa or of a combination of balsa and aluminum-alloy sheet. The aluminum foil was wrapped around this and was largely responsible for the structural strength of the wing. This type of construction produces wing sections which become relatively heavier and stiffer in the outboard portion of the span. The 60° delta wings had a chordwise-grain center lamination with end-grain balsa filling out the airfoil section. In the 45° and 53° 8' delta wings, the center lamination was replaced by the plan-form sheet of 0.020-inch aluminum alloy. Cross sections of these wings are shown in figure 1 with the 60° wings designated type C and the 45° and 53° 8' wings designated type E. A variation of stiffness in the 60° wings was attempted by adding extra thicknesses of foil in the skin but the desired range was not obtained, probably because the adhesive used to attach the foil to the balsa permeated the grain of the wood and contributed so much to the stiffness that the added layers of foil added only a small percentage to the stiffness.

In addition to the built-up wings, a 60° delta wing was built from a magnesium flat plate with beveled edges. The section is shown as type F in figure 1.

Laboratory Measurements

All wings were vibrated and the natural frequencies and nodal patterns up through the sixth vibration mode were determined. Sketches of the plan forms tested are presented in figure 2 and show representative nodal patterns and frequencies for the first four modes. One shaker was used for the determination of the vibration modes and frequencies. As a check, two shakers were used on a few of the wings and also the one shaker was attached at different locations on the wing. When the shakers were kept close to the wing root, there was essentially no difference in the frequencies or nodal patterns obtained. The frequencies obtained with one shaker also agreed with the free-vibration tests which were made to determine structural damping. For the built-up wings, the structural damping varied from 0.02 to 0.03. For the magnesium flat plate, the damping in first bending was 0.007.

Structural influence coefficients were obtained on at least one wing of each type of construction, and for purposes of comparing the stiffness of wings of similar construction the diagonal of the structural-influence-coefficient matrix was determined for all wings tested. The location of the 12 points used for the influence coefficients is shown in the typical loading pattern illustrated in figure 3. The wings were loaded by means of a weighted frame which could be slipped over the wing in such a manner that a load could be applied at the desired point

through a small pad (1/4-inch diameter) which was used to prevent damage to the wing surface. Deflections were measured with dial gages that could be read directly to 0.0001 inch. These dial gages have an accuracy of approximately ±0.0002 inch, well within the scatter of the experimental data. It is probable that, as indicators of small differences, the error is considerably less.

Since there was some question concerning the effect of the dial-gage spring constant on the calculated frequencies and mode shapes, a micrometer which could be read directly to 0.0001 inch was set up on the magnesium wing with a very sensitive electrical contact system. The contact system consisted of a neon lamp connected in series with a 45-volt battery and a 1/4-megohm resistance. One side of this was connected to the wing and the other side to the spindle of the micrometer so that the neon lamp would flash when contact between the micrometer spindle and wing was established. Extremely careful manipulation of the micrometer barrel indicated that a movement of 0.00002 or 0.00003 inch was sufficient to indicate contact or no contact as the case might be and with reasonable care the readings could readily be repeated to the nearest 0.0001 inch. This method was much more time consuming than the dial-gage method but had a significant advantage in that there was no preload or varying load on the wing. When the frequencies and mode shapes were calculated from the influence coefficients determined with the micrometer, they were found to be about 2 percent less in frequency than the values determined from the dial-gage influence coefficients and the difference in mode shape was virtually undetectable.

Vibration frequencies and mode shapes for the first four modes were calculated from the structural influence coefficients. Table I gives the structural influence coefficients, the mode shapes and frequencies calculated from the influence coefficients, the experimentally determined frequencies, and the calculated mass of the wing segments associated with the loading stations shown in figure 3. The structural-influence-coefficient data are the original data with no adjustment made in order to conform to Maxwell's theorem of reciprocity, since, in earlier calculations, where both the symmetrical and unsymmetrical matrices were employed, it was found that the same or slightly better agreement of the calculated with the experimental values of frequency were obtained with the unsymmetrical matrix. Only the first three modes are presented because it is felt that with only 12 load points a calculated fourth mode is somewhat meaningless. Generally, the calculated fourth mode did not agree too well with the experimental value of frequency or nodal pattern. Mode shapes were not measured experimentally, but the node lines determined from the calculated mode shapes for the first three modes seem to be in reasonable agreement with the experimentally determined node lines.

Pertinent wing parameters are listed in table II. The values listed in table II are associated with the free-stream root section. Also, inasmuch as a delta wing has no elastic axis in the commonly accepted sense of the term, the value listed for x_o is for a reference axis and is assumed based on consideration of the structural characteristics of the free-stream section. Since, on a few of the wings, certain parameters vary with span, the spanwise variation of these parameters is listed in table III, which also lists the bending and torsion mode shapes. It should be pointed out that the mode shapes listed in table III are in a different form from the mode shapes listed in table I. The mode shapes in table III are derived from the mode shapes calculated from the influence coefficients and have been adjusted so that they lend themselves more readily to the flutter calculations which will be discussed later in this paper. The mode shapes given are the mode shapes of the wing considered as a beam extending perpendicular to the airstream with a span equal to the span of the wing and are derived in the following manner. For the bending mode, the normalized values from table I for the three chordwise points at each of the four spanwise stations (see fig. 3) were averaged and a curve of displacement against span faired through the resulting four spanwise points. This curve was extrapolated to the wing tip and the normalized values in table III were obtained from this curve. For the torsion mode, a similar method was used in that the slope indicated by the three chordwise points at each spanwise station was approximated by a straight line. The slope of each of these lines was determined and a curve of slope against span faired through these points and extrapolated to the tip. The values of slope at the desired stations were then normalized and are listed in table III as the torsion mode.

Instrumentation and Test Technique

All wings were instrumented with four 4-arm strain-gage bridges attached in pairs. Each pair was oriented so that one bridge would read flexural strain along an arbitrary axis and the second bridge would read the torsional strain at an angle of 45° to that axis. The output from these gages was recorded on a recording oscillograph for part of the tests and on a multichannel tape recorder for the remainder of the tests. The beginning of flutter and the flutter frequency can be determined from these records.

In some cases the output from one of the strain-gage bridges was fed into a sensing device which triggered high-speed flash lamps at the maximum strain points of a cycle of flutter. This method yields a double-exposure photograph which gives a good qualitative delineation of the flutter mode. Two of these high-speed flash photographs taken of wing 13 and wing 14 are shown in figure 4. A similar system for determining static vibration modes, triggered by an amplitude-sensing device, is reported in reference 6.

Since in many cases the onset of flutter was both sudden and violent, a system was set up that enabled the tunnel operator to record desired information automatically. By closing one switch, (1) an oscillograph record could be obtained, (2) test point number, test-section Mach number, static pressure, and stagnation temperature could be recorded on an electric typewriter by the tunnel read-out system and (3) a short burst of high-speed movies and the high-speed flash photographs could be obtained. In some cases the onset of flutter was so abrupt and wing failure so rapid that it was found necessary to run the recorder continuously in order to obtain a record of the oscillations before the wing failed. Figure 5 presents a record of this type. The read-out signal in the third line from the bottom indicates the time when the switch was closed. Since conditions change slowly in the tunnel, the difference in time between wing flutter and the time when the data were recorded is felt to be negligible.

Usually flutter was obtained at the desired Mach number by increasing the speed of the tunnel at reduced density and then increasing the tunnel density until flutter occurred.

Test Facility

The tests were performed in the Langley 8-foot transonic pressure tunnel. For the flutter tests, a reflection plane was installed in the tunnel and all wings were attached with mounting brackets to this reflection plane as semispan cantilevers. A fairing was attached to the wing-mounting brackets to smooth out the flow over the inboard section of the wing. A schematic downstream section view of a wing mounted in the tunnel is shown in figure 6. A photograph of a wing installed in the tunnel is shown in figure 7.

The reflection plane was a 1-inch-thick steel plate whose primary support was a circular-arc steel strut 5 inches thick. This strut was attached to the tunnel and to the center of the reflection plane. In order to eliminate any possibility of yaw and roll of the plane, 17 auxiliary supports in the form of small streamlined struts were attached to the tunnel wall and the reflection plane at various points. In view of the method of attachment and the mass of the plane, it is felt that the wings were attached to a virtually rigid body and that the assumption of a true cantilever mount is valid.

The reflection plane served to bleed off the boundary layer and to move the test wings out of the tunnel boundary layer which was approximately 3.5 inches thick just ahead of the leading edge of the plane. The boundary layer at the center of the plate was approximately 0.8 inch. The Mach number gradient with the plane in the tunnel was small with a maximum Mach number deviation below $M = 1.0$ of ± 0.005 occurring at

M = 0.99. Above M = 1.0 the flow deteriorated, probably due to reflection of shocks originating at the reflection plane leading edge. For this reason no flutter data are presented for Mach numbers in excess of 1.02. No complete survey has been made of flow angularity but tuft studies indicate no angularity except on the top and bottom of the reflection-plane trailing edge.

TEST RESULTS

Flutter has been obtained on three delta-wing plan forms, 60°, 53° 8', and 45° leading-edge sweepback, at Mach numbers from 0.4 to 1.00. The mass ratio μ of the tests varied from 7 for the lighter wings at the higher densities to 85 for the heavier wings at the lower densities. Experimental data, including Mach number, test density, mass ratio, flutter velocity, and other pertinent information, are listed in table IV.

For the 60° delta wings, with the exception of the magnesium flat plate, the test Mach numbers ranged from 0.6 to 1.1. Flutter was obtained from M = 0.7 to M = 1.0. The mass ratio for these tests ranged from 7 to 40. Figure 8(a) shows a plot of q against Mach number for the 60° foil-covered wings. Figure 8(b) shows a plot of q against Mach number for the 60° magnesium flat plate. The 60° flat plate fluttered over a range of Mach numbers from 0.4 to 1.1 at values of μ from 8 to 34. In the lower Mach number range, it was possible to flutter the wing in two modes, depending on the test technique, with the higher mode flutter occurring at the lower values of density. The frequencies given in the key are the flutter frequencies.

For the 53° 8' delta wings, flutter was obtained over a Mach number range from 0.5 to 0.9. For the spruce wings there was a marked Mach number effect which decreased the value of q necessary to avoid flutter at M = 0.9 to a value that could not be obtained in the tunnel because of a minimum density limitation. Consequently, no flutter was obtained on this wing at the higher Mach numbers. The values of μ of the tests ranged from 14 at the low Mach numbers to 75 at the high Mach numbers. Figure 8(c) shows a plot of q against Mach number for the 53° 8' wings.

The tests of the 45° model were inconclusive. Although a number of tests were made on this plan form, only one discrete flutter point was obtained. This point was for the foil-covered wing (wing 12) and resulted in failure; therefore, flutter at other Mach numbers could not be obtained. It may be seen from the high-speed flash photographs shown in figure 9 that the oscillation of the 45° spruce wing (wing 11) involved a large amount of camber. Since the instrumentation was not designed to respond to stresses in the chordwise direction, the actual

character of these oscillations could not be too well determined from the strain-gage signals. It was also difficult to determine a definite flutter point. The difficulty in this respect was that the wing would start a sustained low-amplitude oscillation at low speed or density and the amplitude would build up gradually as the speed or the density was increased - much as though the wing were being forced by a vibrator. Consequently, the data presented in table III for this wing (wing 11) should be used with caution. In addition, the wing seemed to respond in different modes at random, although the higher modes occurred predominately at the higher values of dynamic pressure.

DISCUSSION OF EXPERIMENTAL DATA

Perusal of the test results reveals several points of interest. Figure 10(a) shows a plot of the nondimensional stiffness-altitude coefficient $\frac{b_r\omega_\alpha}{V_c}\sqrt{\mu_{e,r}}$ against Mach number for the 60° delta wings, except the flat plate. In this plot, constant altitude would be indicated by a straight horizontal line and constant dynamic pressure, by a straight line through the origin. In addition to the tests made in the 8-foot transonic pressure tunnel, results obtained in the Langley supersonic flutter apparatus at $M = 1.3$ on a wing with a similar frequency spectrum are also placed in this figure in order to extend the curves to supersonic Mach numbers. With one exception, these wings fluttered at frequencies lower than either second bending or torsion. With the stiffness-altitude coefficient used as a basis of comparison, it is obvious that the wings with the second bending frequency lower than the torsion frequency are more likely to flutter than wings for which the opposite is true. It is interesting to note that for these 60° delta wings, over the range of Mach number considered, that the transonic range is apparently the critical flutter region as was the case for the unswept and swept wings reported in references 1 and 2.

Figure 10(b) shows a plot of the stiffness-altitude coefficient against Mach number for the 60° delta flat plate (wing 10). This configuration is felt to be of interest since its mechanical properties can be easily duplicated or scaled for possible comparison or extension to other Mach number ranges in other facilities. In order to extend the range to higher Mach numbers, a test point from reference 8 is shown at $M = 1.3$. Reference 8 uses the third mode as ω_α but since the third mode of wing 10 was not a clear torsional vibration the second mode was used as a reference frequency and the point taken from reference 8 has been adjusted accordingly.

Figure 10(c) shows a plot of stiffness-altitude coefficient against Mach number for the 53° 8' delta wings. Although the limitation of the minimum operating density of the tunnel prevented obtaining flutter information above a Mach number of 0.9, there is apparently a much more pronounced Mach number effect in the transonic region than for 60° delta wings. In addition to the tests made in the 8-foot transonic pressure tunnel, results obtained in the Langley supersonic flutter apparatus on a wing with a similar frequency spectrum are placed in the figure to extend the curve into the supersonic range. This test point indicates that the curve does turn back as in the case of the 60° delta wing. A comparison between the 53° 8' wings with the different frequency spectra may not be completely justified since the wings with the torsional frequency lower than the second bending frequency fluttered at higher frequencies, relative to the natural frequency spectrum, than the wing for which the opposite is true. There is, however, a definite difference in the flutter boundary for the two wings. The trend found in the 60° wings, that is, that the wing with second bending frequency lower than torsion frequency is more likely to flutter, is reversed for the 53° 8' delta wings. The reason for this anomaly is not known.

It is interesting to note that for both the 60° and 53° 8' plan forms, the wing more likely to flutter had the torsion node line farther back on the wing tip.

COMPARISON OF EXPERIMENTAL WITH CALCULATED RESULTS

As a means of normalizing the flutter data obtained on the various wings, simplified flutter-speed calculations based on the method of reference 7 have been made on a few sample cases. This flutter speed V_R is calculated on the basis of two-dimensional flow (strip analysis) with the effect of mode shape and the angle of sweep included. Aerodynamic coefficients for two-dimensional incompressible flow were employed in conjunction with two degrees of freedom (first natural bending and first natural torsion). The frequencies used were the frequencies obtained in the vibration tests of the wings. The air density used was that at the start of sustained flutter. The sections considered for the geometric, mass, and inertia parameters were the streamwise sections and the mode shape taken perpendicular to the free stream; therefore, in these respects the sweep angle of the leading edge did not enter into the calculation. On the other hand, in the various terms of the flutter-determinant elements, where the sweep angle or some function thereof was required, the sweep angle of the leading edge was employed. For example, consider the A_2-term of equation (19a) of reference 7. (See the equation after eq. (206) of ref. 7.) This may be rewritten as follows:

[redacted]

$$K_1 \frac{l'}{b_r} A + K_2 \left(i \frac{1}{k_n} \right) \left(\left[-1 \right] + A_{ch} \right) \tan \Lambda - \left[K_3 \frac{\tan^2 \Lambda}{l'} \frac{1}{b_1} \frac{1}{k_n^2} \right]$$

where K_1, K_2, and K_3 are constants depending on the mode shape, l' is length taken perpendicular to free stream, b_r is the root semichord taken in the free-stream direction, Λ is the sweep angle of the leading edge, k_n is based on the free-stream semichord and the velocity over the wing in the free-stream direction, A is defined in reference 7, and A_{ch} is based on values of F and G which are functions (of k_n) associated with the wake developed by Theodorsen in reference 9. The terms in the special bracket $\left[\ \right]$ are often neglected.

After the flutter-speed coefficient $V/b\omega_\alpha$ was solved for the velocity V the reciprocal of the cosine of the leading-edge sweep angle was used as a multiplying factor to obtain the value of V_R listed in table IV.

In view of the simplifying assumptions made, the reference flutter-speed calculation should not be expected to predict accurately an experimental flutter speed. Rather, it may be considered as a common denominator which serves to eliminate in part the effect of certain wing parameters in order that the data presented may be made more general.

The results of the flutter-speed calculations are presented in figure 11 as a plot of V_e/V_R against Mach number. It may be seen that, for the majority of the test points, the ratio is less than 1.0, which means that the calculated value is unconservative but becomes more conservative with increase in Mach number. The calculations indicate the same trend as that found for unswept and swept wings (refs. 1 and 3); that is, over the range investigated, the calculations tend to become more conservative at Mach numbers above $M = 0.9$, but there are not sufficient data to allow a positive statement in this regard. In two cases (wings 1 and 9), calculations were made using three modes - first bending, second bending, and torsion. In one of these (wing 1), the addition changed the value obtained by only 5 percent although the experimental flutter frequency was almost the same as the second bending frequency (third mode) of the wing. For the other calculation (wing 9), the addition of the second bending mode (second mode) increased the calculated value by about 50 percent and resulted in excellent agreement with experiment.

A simpler method for determining calculated speeds is presented in reference 4 in the form of an empirically derived criterion. This may

be used as an alternate method if the required stiffness data are available. This criterion is presented below:

$$V_1 = \left(\frac{m_\theta}{\rho_o s c_m^2}\right)^{1/2} \frac{(0.9 - 0.33k)\left(0.77 + \frac{0.1}{r}\right)\left(0.95 + \frac{0.1}{\sigma_w}\right)}{0.78(g - 0.1)} \sec^{3/2}\left(\Lambda - \frac{\pi}{16}\right)$$

$$V_2 = V_1\left(1 - 0.166M_1 \cos \Lambda\right) \qquad M_1 = V_1/a$$

where

a velocity of sound, fps

m_θ torsional stiffness measured at 0.7 span, ft-lb/radian

ρ_o test density, slugs/cu ft (ρ_o same as ρ_e of this paper)

s exposed semispan, ft

c_m mean chord, ft

k taper ratio (Tip chord/Root chord)

r stiffness ratio, $l_\phi c_m^2/0.81 m_\theta s^2$

l_ϕ flexural stiffness measured at 0.7 span, ft-lb/radian

σ_w wing density, $\frac{\text{Weight of wing}}{s c_m^2}$, lb/cu ft

Λ leading-edge sweepback, radians

g section center of gravity in fraction of chord

For this criterion, as in the case of V_R, the calculated speeds were generally somewhat unconservative. The criterion also seemed to break down when higher modes were involved in the flutter or when the density at flutter was much less than two-thirds standard atmosphere. A density correction $\sqrt[4]{\frac{0.000238}{\rho_e}}$ used as a multiplying factor for the flutter speed predicted by the criterion improved the agreement with experiment. The calculated values of the predicted flutter speed are listed in table IV.

[redacted]

SUMMARY OF RESULTS

Flutter tests have been made in the high subsonic and transonic speed range on delta-wing plan forms with leading-edge sweepbacks of 60°, 53° 8', and 45° at Mach numbers M from 0.4 to 1.0. The following results were noted:

1. One result of the 60° tests was that, for comparable wings (that is, approximately equal size, torsional frequency, and weight), the ratio of second bending frequency to the torsional frequency had a marked effect on the flutter velocity, the wings with the value of the ratio less than 1.0 being more likely to flutter than the wings for which the opposite was true.

2. For the 53° 8' wings, there was a marked effect in a direction opposite to that for the 60° wings, but a comparison may not be justified since the wings with the different frequency ratios fluttered in different flutter modes.

3. There was a marked compressibility effect on both the 60° and the 53° 8' delta wings in that both plan forms were more susceptible to flutter in the low transonic region (M = 0.9 to 1.0) than in the high subsonic range (M = 0.7 to 0.85). This condition changed rapidly in the case of the 60° delta wing and the indication is that at Mach numbers slightly over 1.0 the likelihood of flutter is greatly reduced. This result leads to the conclusion, previously drawn for unswept and swept wings, that for a given altitude over the range investigated, the transonic region is the region where flutter is most likely to occur.

4. Simplified flutter calculations involving two-dimensional incompressible coefficients, two modes (first bending and first torsion), and sweep have been made for a few cases and generally the answers derived from the calculations are somewhat unconservative although in four of the cases calculated the reverse is true.

5. The addition of the third mode (second bending) to two of the cases calculated made very little difference in one of the answers obtained although the flutter frequency was very close to the second bending frequency. In the second calculation, the calculated speed was increased by about 50 percent and agreed very well with the experimental value.

6. The calculations indicate the same trend with Mach number as that found for swept and unswept wings; that is, over the range investigated, the calculations tend to become more conservative at Mach numbers above M = 0.9 but there are not sufficient data to allow a positive statement in this regard.

[redacted]

7. A comparison has been made of experimental flutter speed with speeds obtained from an empirically derived criterion which involves test density and geometric, stiffness, and mass characteristics of the plan form. The predicted speed was generally somewhat unconservative and apparently the criterion is not applicable at low test densities or to flutter involving higher modes.

Langley Aeronautical Laboratory,
National Advisory Committee for Aeronautics,
Langley Field, Va., Nov. 9, 1956.

[redacted]

1. Lauten, William T., Jr., and Barmby, J. G.: Continuation of Wing Flutter Investigation in the Transonic Range and Presentation of a Limited Summary of Flutter Data. NACA RM L9B25b, 1949.

2. Lauten, William T., Jr., and O'Kelly, Burke R.: Free-Flight Flutter Tests in the Transonic and Low Supersonic Speed Range of Three Low-Aspect-Ratio, Swept, Tapered Wings on Rocket-Propelled Vehicles. NACA RM L55J21, 1956.

3. Unangst, John R., and Jones, George W., Jr.: Some Effects of Sweep and Aspect Ratio on the Transonic Flutter Characteristics of a Series of Thin Cantilever Wings Having a Taper Ratio of 0.6. NACA RM L55I13a, 1956.

4. Molyneux, W. G., and Ruddlesden, F.: Flutter Tests on Some Delta Wings Using Ground Launched Rockets. Rep. No. Structures 173, British R.A.E., Feb. 1955.

5. Jones, George W., Jr., and Young, Lou S., Jr.: Transonic Flutter Investigation of Two 64° Delta Wings With Simulated Streamwise Rib and Orthogonal Spar Construction. NACA RM L56I27, 1957.

6. Herr, Robert W.: A Preliminary Wind-Tunnel Investigation of Flutter Characteristics of Delta Wings. NACA RM L52B14a, 1952.

7. Barmby, J. G., Cunningham, H. J., and Garrick, I. E.: Study of Effects of Sweep on the Flutter of Cantilever Wings. NACA Rep. 1014, 1951. (Supersedes NACA TN 2121.)

8. Tuovila, W. J., and McCarty, John Locke: Experimental Flutter Results for Cantilever-Wing Models at Mach Numbers Up to 3.0. NACA RM L55E11, 1955.

9. Theodorsen, Theodore: General Theory of Aerodynamic Instability and the Mechanism of Flutter. NACA Rep. 496, 1935.

[redacted]

TABLE I.- STRUCTURAL INFLUENCE COEFFICIENTS AND

RELATED INFORMATION AS INDICATED IN FIGURE 3

(a) Wing 1

Loading station	Deflections for a 6-lb load, in inches, at loading station -											
	1	2	3	4	5	6	7	8	9	10	11	12
1	0.7270	0.1636	0.0211	0.0024	0.6639	0.2399	0.0660	0.0053	0.6645	0.2434	0.0865	0.0053
2	.1729	.1306	.0235	.0037	.1396	.0880	.0367	.0045	.1030	.0513	.0155	.0006
3	.0370	.0401	.0199	.0028	.0166	.0119	.0066	.0013	.0129	.0045	.0008	.0000
4	.0024	.0037	.0028	.0012	.0005	.0009	.0004	.0000	.0002	.0000	.0000	.0000
5	.6639	.1396	.0166	.0005	.7337	.2365	.0431	.0032	.6505	.2322	.0576	.0066
6	.2399	.0880	.0119	.0009	.2365	.1356	.0308	.0016	.1835	.0943	.0292	.0028
7	.0660	.0367	.0066	.0004	.0431	.0308	.0176	.0003	.0446	.0251	.0087	.0000
8	.0053	.0045	.0013	.0000	.0032	.0016	.0003	.0008	.0009	.0011	.0007	.0000
9	.6645	.1030	.0129	.0002	.6508	.1835	.0446	.0009	1.0192	.3195	.0770	.0079
10	.2434	.0513	.0045	.0000	.2322	.0943	.0251	.0011	.3195	.2560	.0749	.0085
11	.0865	.0155	.0008	.0000	.0576	.0292	.0087	.0007	.0770	.0749	.0581	.0085
12	.0053	.0006	.0000	.0000	.0066	.0028	.0000	.0000	.0079	.0085	.0085	.0045

Loading station	H_{h_1}	H_{h_2}	H_{α}	Mass of numbered segments (indicated by dashed lines in fig. 3), lb-sec^2/in.
1	0.9905	-0.5190	0.0423	0.4048×10^{-4}
2	.2796	.3444	.7207	1.7449
3	.0516	.1397	.2837	4.1763
4	.0036	.0175	-.0320	7.9762
5	.9587	-1.0000	.0564	.4970
6	.3859	.0837	.3406	2.1426
7	.1014	.1544	.1837	5.1293
8	.0068	.0144	.0246	9.7962
9	1.0000	-.8988	-1.0000	.2661
10	.4536	.7082	-.6970	1.2213
11	.1434	.4749	-.2785	2.7463
12	.0143	.0688	-.0490	4.8454
$f_{calc.}$, cps . . .	34.0	85.0	72.5	
$f_{exp.}$, cps . . .	29.8	88.0	78.0	

TABLE I.- STRUCTURAL INFLUENCE COEFFICIENTS AND RELATED INFORMATION

AS INDICATED IN FIGURE 3 - Continued

(b) Wing 3

Loading station	Deflections for a 6-lb load, in inches, at loading station -											
	1	2	3	4	5	6	7	8	9	10	11	12
1	0.2391	0.0636	0.0105	0.0000	0.1989	0.0776	0.0177	0.0015	0.1617	0.0680	0.0264	0.0042
2	.0871	.0743	.0199	.0016	.0683	.0452	.0159	.0018	.0500	.0234	.0086	.0014
3	.0145	.0198	.0175	.0020	.0101	.0089	.0049	.0008	.0044	.0014	.0004	.0000
4	.0000	.0013	.0018	.0016	.0002	.0005	.0003	.0001	.0000	.0000	.0000	.0000
5	.2022	.0504	.0080	.0000	.2225	.0736	.0168	.0012	.2178	.0921	.0364	.0058
6	.0991	.0440	.0090	.0004	.0955	.0623	.0183	.0018	.0889	.0502	.0218	.0028
7	.0235	.0153	.0048	.0002	.0219	.0176	.0127	.0015	.0178	.0110	.0056	.0010
8	.0009	.0011	.0005	.0000	.0008	.0013	.0016	.0010	.0002	.0003	.0002	.0000
9	.1662	.0400	.0048	.0000	.2262	.0687	.0153	.0006	.3159	.1212	.0460	.0036
10	.0691	.0178	.0018	.0000	.0924	.0392	.0090	.0003	.1182	.0888	.0388	.0062
11	.0340	.0090	.0010	.0000	.0469	.0218	.0059	.0005	.0562	.0507	.0379	.0071
12	.0045	.0009	.0000	.0000	.0066	.0034	.0009	.0001	.0063	.0069	.0062	.0037

Loading station	H_{h_1}	H_{h_2}	H_{α}	Mass of numbered segments (indicated by dashed lines in fig. 3), lb-sec^2/in.
1	0.9360	-1.0000	0.1083	0.3789×10^{-4}
2	.4945	.1410	.9426	1.6333
3	.1083	.2232	.4728	3.9091
4	.0061	.0328	.0459	7.4659
5	.9651	-.8465	-.4281	.4854
6	.5883	.0856	.1993	2.0928
7	.1708	.1928	.2103	5.0101
8	.0112	.0311	.0310	9.5686
9	1.0000	-.6992	-1.0000	.2269
10	.5187	.3572	-.7126	1.0411
11	.3041	.5868	-.5367	2.3411
12	.0442	.1184	-.0911	4.4712
$f_{calc.}$, cps . . .	58.0	141.0	104.0	
$f_{exp.}$, cps . . .	51.0	142.0	115.0	

TABLE I.- STRUCTURAL INFLUENCE COEFFICIENTS AND RELATED INFORMATION

AS INDICATED IN FIGURE 3 - Continued

(c) Wing 4

Loading station	Deflections for a 8-lb load, in inches, at loading station -											
	1	2	3	4	5	6	7	8	9	10	11	12
1	0.3872	0.0908	0.0096	0.0000	0.4144	0.1600	0.0412	0.0020	0.4504	0.2098	0.0740	0.0076
2	.0911	.0603	.0116	.0000	.0881	.0572	.0239	.0020	.0827	.0498	.0215	.0025
3	.0100	.0113	.0105	.0004	.0078	.0071	.0049	.0010	.0056	.0029	.0013	.0001
4	.0000	.0001	.0004	.0013	.0000	.0000	.0001	.0000	.0000	.0000	.0000	.0000
5	.4140	.0864	.0080	.0000	.4900	.1692	.0416	.0016	.5476	.2544	.0872	.0096
6	.1601	.0582	.0072	-.0001	.1707	.0909	.0271	.0015	.1766	.1085	.0462	.0051
7	.0397	.0235	.0054	.0000	.0409	.0266	.0137	.0011	.0396	.0262	.0132	.0020
8	.0022	.0023	.0013	.0000	.0018	.0015	.0012	.0009	.0009	.0006	.0005	.0001
9	.4412	.0836	.0064	.0000	.5596	.1800	.0400	.0016	.6856	.2912	.0994	.0104
10	.2100	.0484	.0036	.0000	.2552	.1080	.0268	.0008	.2860	.1884	.0732	.0084
11	.0762	.0204	.0012	.0000	.0948	.0476	.0136	.0004	.0964	.0736	.0456	.0064
12	.0085	.0026	.0002	.0000	.0115	.0059	.0021	.0001	.0107	.0088	.0068	.0037

Loading station	H_{h_1}	H_{h_2}	H_{α}	Mass of numbered segments (indicated by dashed lines in fig. 3), lb-sec^2/in.
1	0.77557	-0.14177	0.96284	0.5062×10^{-4}
2	.21323	.57982	.41627	1.9015
3	.02404	.10219	.21771	4.4000
4	.00013	.00391	.00541	8.2852
5	.88835	-.56079	.77307	.6014
6	.37254	.32116	-.09945	2.4942
7	.10159	.26402	.03355	5.8883
8	.00522	.03719	.03409	11.1731
9	1.00000	-1.00000	.73880	.3173
10	.52539	-.14944	-1.00000	1.2071
11	.21191	.07294	-.90077	2.6175
12	.02644	.02086	-.16494	4.8997
$f_{calc.}$, cps . . .	42.0	112.0	142.0	
$f_{exp.}$, cps . . .	36.0	105.0	131.0	

TABLE I.- STRUCTURAL INFLUENCE COEFFICIENTS AND RELATED INFORMATION

AS INDICATED IN FIGURE 3 - Continued

(d) Wing 7

Loading station	Deflections for a 8-lb load, in inches, at loading station -											
	1	2	3	4	5	6	7	8	9	10	11	12
1	0.3312	0.0744	0.0092	0.0000	0.3580	0.1148	0.0325	0.0030	0.3264	0.1604	0.0612	0.0108
2	.0764	.0453	.0104	.0001	.0618	.0432	.0199	.0025	.0600	.0353	.0183	.0030
3	.0087	.0104	.0091	.0004	.0067	.0040	.0050	.0013	.0050	.0017	.0012	.0002
4	.0000	.0001	.0004	.0015	.0000	-.0004	.0000	.0000	-.0012	-.0010	-.0008	.0000
5	.3580	.0624	.0076	.0000	.4416	.1212	.0316	.0012	.4325	.1904	.0696	.0108
6	.1284	.0432	.0066	-.0004	.1298	.0705	.0228	.0017	.1252	.0806	.0409	.0056
7	.0300	.0199	.0050	.0000	.0302	.0216	.0123	.0014	.0265	.0200	.0128	.0027
8	.0030	.0023	.0013	.0000	.0012	.0017	.0014	.0012	.0016	.0012	.0008	.0002
9	.3264	.0596	.0052	-.0012	.4588	.1232	.0332	.0016	.6560	.2288	.0788	.0140
10	.1600	.0353	.0032	-.0010	.1800	.0792	.0200	.0012	.2000	.1508	.0612	.0111
11	.0612	.0183	.0012	-.0008	.0672	.0409	.0128	.0008	.0804	.0580	.0408	.0096
12	.0108	.0030	.0002	.0000	.0100	.0056	.0027	.0002	.0140	.0111	.0096	.0060

Loading station	H_{h_1}	H_{h_2}	H_{α}	Mass of numbered segments (indicated by dashed lines in fig. 3), lb-sec^2/in.
1	0.1707	-0.2205	0.9557	0.4764×10^{-4}
2	.1983	.3515	.5230	1.7352
3	.0237	.1022	.2612	4.1104
4	-.0019	-.0018	.0358	7.6153
5	.8927	-.6178	.7360	.5429
6	.3528	.2832	.0576	2.2400
7	.0984	.2149	.1010	5.4012
8	.0076	.0301	.0383	10.1353
9	1.0000	-1.0000	-.1011	.2946
10	.4847	.1141	-1.0000	1.1181
11	.2136	.2204	-.6839	2.5362
12	.0382	.0565	-.2301	4.6352
$f_{calc.}$, cps . . .	49.0	116.0	145.0	
$f_{exp.}$, cps . . .	40.0	105.0	139.0	

TABLE I.- STRUCTURAL INFLUENCE COEFFICIENTS AND RELATED INFORMATION

AS INDICATED IN FIGURE 3 - Continued

(e) Wing 3

Loading station	Deflections for a 9-lb load, in inches, at loading station -											
	1	2	3	4	5	6	7	8	9	10	11	12
1	0.3168	0.0639	0.0075	0.0000	0.3354	0.1206	0.0321	0.0024	0.3480	0.1620	0.0567	0.0072
2	.0660	.0437	.0091	.0001	.0634	.0399	.0183	.0023	.0597	.0369	.0163	.0024
3	.0080	.0095	.0088	.0004	.0067	.0057	.0044	.0012	.0042	.0027	.0012	.0001
4	.0000	.0002	.0006	.0012	.0000	.0000	.0001	.0001	.0000	.0000	.0000	.0000
5	.3378	.0609	.0063	.0000	.4137	.1245	.0318	.0024	.4671	.1980	.0669	.0084
6	.1204	.0402	.0057	.0000	.1274	.0660	.0209	.0019	.1338	.0831	.0361	.0050
7	.0312	.0176	.0042	.0001	.0320	.0209	.0115	.0014	.0312	.0227	.0108	.0020
8	.0026	.0024	.0012	.0000	.0022	.0016	.0013	.0009	.0014	.0010	.0006	.0001
9	.3555	.0582	.0048	-.0003	.4725	.1323	.0321	.0018	.6201	.2361	.0680	.0099
10	.1620	.0369	.0027	.0000	.1977	.0846	.0210	.0012	.2307	.1512	.0594	.0081
11	.0576	.0174	.0015	.0000	.0690	.0363	.0108	.0006	.0786	.0645	.0393	.0063
12	.0083	.0028	.0001	.0000	.0085	.0045	.0020	.0001	.0110	.0098	.0065	.0040

Loading station	H_{h_1}	H_{h_2}	H_{α}	Mass of numbered segments (indicated by dashed lines in fig. 3), lb-sec^2/in.
1	0.74164	-0.18903	0.96926	0.4490×10^{-4}
2	.18570	.40802	.67794	1.9176
3	.02397	.13691	.32703	4.4264
4	.00022	.00523	.01521	8.3170
5	.86805	-.59646	.65473	.5738
6	.33782	.27895	.05993	2.4581
7	.09821	.21707	.16009	5.8028
8	.00731	.03330	.06589	10.9984
9	1.00000	-1.00000	.22211	.3077
10	.50532	.06372	-1.00000	1.2633
11	.20701	.20462	-.91149	2.7515
12	.03005	.01390	-.19288	5.1503
$f_{calc.}$, cps . . .	50.2	127.0	155.0	
$f_{exp.}$, cps . . .	42.0	111.0	148.0	

TABLE I.- STRUCTURAL INFLUENCE COEFFICIENTS AND RELATED INFORMATION

AS INDICATED IN FIGURE 3 - Continued

(f) Wing 11

Loading station	Deflections for a 15-lb load, in inches, at loading station -											
	1	2	3	4	5	6	7	8	9	10	11	12
1	0.1911	0.0585	0.0162	0.0018	0.1614	0.0564	0.0153	0.0021	0.1395	0.0456	0.0111	0.0012
2	.0594	.0429	.0141	.0016	.0478	.0260	.0094	.0016	.0426	.0169	.0050	.0004
3	.0156	.0136	.0108	.0017	.0136	.0089	.0038	.0007	.0117	.0050	.0014	.0001
4	.0015	.0015	.0017	.0011	.0016	.0011	.0006	.0001	.0008	.0004	.0000	.0000
5	.1602	.0495	.0135	.0015	.1743	.0575	.0159	.0021	.1755	.0573	.0159	.0018
6	.0558	.0478	.0082	.0009	.0561	.0310	.0105	.0019	.0575	.0304	.0098	.0012
7	.0161	.0092	.0039	.0005	.0165	.0117	.0063	.0013	.0176	.0105	.0039	.0006
8	.0027	.0017	.0007	.0001	.0025	.0021	.0014	.0006	.0026	.0019	.0009	.0002
9	.1314	.0420	.0114	.0009	.1746	.0579	.0171	.0025	.2472	.0753	.0207	.0024
10	.0462	.0165	.0048	.0003	.0585	.0309	.0104	.0018	.0762	.0705	.0237	.0033
11	.0117	.0045	.0014	.0001	.0161	.0103	.0041	.0007	.0210	.0242	.0227	.0036
12	.0013	.0004	.0001	.0000	.0022	.0014	.0005	.0001	.0027	.0034	.0035	.0027

Loading station	H_{h_1}	H_{h_2}	H_{α}	Mass of numbered segments (indicated by dashed lines in fig. 3), lb-sec^2/in.
1	0.9462	-0.7394	0.6903	1.6632×10^{-4}
2	.4089	.3276	.5691	9.1503
3	.1382	.2661	.2630	20.2021
4	.0164	.0464	.0435	35.4197
5	.9590	-.8578	.1984	2.1269
6	.4264	.0930	.0251	11..1036
7	.1506	.1311	-.0025	25.0596
8	.0273	.0372	-.0050	44.6891
9	1.0000	-1.0000	-.3735	.9430
10	.4864	.1284	-1.0000	5.6891
11	.1718	.2551	-.6572	12.1373
12	.0236	.0434	-.1154	20.9870
$f_{calc.}$, cps . . .	48.9	115.0	94.3	
$f_{exp.}$, cps . . .	45.5	90.0	108.0	

TABLE I.- STRUCTURAL INFLUENCE COEFFICIENTS AND RELATED INFORMATION

AS INDICATED IN FIGURE 3 - Continued

(g) Wing 12

Loading station	Deflections for a 14-lb load, in inches, at loading station -											
	1	2	3	4	5	6	7	8	9	10	11	12
1	0.7571	0.2331	0.0441	0.0018	0.7963	0.3045	0.0812	0.0088	0.7831	0.3448	0.1061	0.0126
2	.2365	.1403	.0350	.0017	.2359	.1409	.0507	.0063	.2309	.1400	.0521	.0068
3	.0427	.0340	.0216	.0021	.0409	.0300	.0164	.0031	.0377	.0245	.0111	.0015
4	.0008	.0015	.0018	.0017	.0007	.0012	.0007	.0003	.0002	.0007	.0002	.0000
5	.7875	.2345	.0420	.0014	.8728	.3178	.0833	.0088	.9202	.3843	.1162	.0147
6	.3135	.1406	.0308	.0012	.3256	.1746	.0562	.0063	.3276	.1984	.0744	.0100
7	.0795	.0497	.0168	.0010	.0832	.0551	.0260	.0036	.0810	.0565	.0298	.0052
8	.0082	.0068	.0037	.0005	.0086	.0070	.0040	.0015	.0079	.0066	.0037	.0007
9	.7949	.2296	.0392	.0007	.9317	.3318	.0833	.0084	1.0654	.4039	.1246	.0161
10	.3427	.1316	.0252	.0007	.3892	.1974	.0567	.0060	.4022	.2695	.0942	.0130
11	.1043	.0511	.0112	.0002	.1168	.0740	.0296	.0032	.1210	.0945	.0626	.0105
12	.0113	.0063	.0014	.0000	.0134	.0098	.0048	.0006	.0141	.0129	.0101	.0057

Loading station	H_{h_1}	H_{h_2}	H_{α}	Mass of numbered segments (indicated by dashed lines in fig. 3), lb-sec^2/in.
1	0.8762	-0.5147	0.6963	2.0393×10^{-4}
2	.3266	.4398	.7435	7.0067
3	.0676	.2074	.4375	14.5990
4	.0024	.0155	.0442	25.0951
5	.9525	-.7495	.1680	2.2738
6	.4234	.3218	.0005	8.1435
7	.1256	.2672	.1006	17.5391
8	.0145	.0466	.0445	28.9886
9	1.0000	-1.0000	-.2481	1.5391
10	.4956	.2506	-1.0000	4.7744
11	.1742	.3219	-.7111	9.5433
12	.0230	.0628	-.1518	16.1013
$f_{calc.}$, cps . . .	20.9	57.5	84.0	
$f_{exp.}$, cps . . .	21.0	52.5	77.0	

TABLE I.- STRUCTURAL INFLUENCE COEFFICIENTS AND RELATED INFORMATION

AS INDICATED IN FIGURE 3 - Continued

(h) Wing 14

Loading station	Deflections for a 12-lb load, in inches, at loading station -											
	1	2	3	4	5	6	7	8	9	10	11	12
1	0.1986	0.0532	0.0114	0.0005	0.1574	0.0574	0.0159	0.0022	0.1257	0.0464	0.0132	0.0017
2	.0527	.0440	.0131	.0008	.0412	.0242	.0095	.0014	.0308	.0124	.0038	.0001
3	.0123	.0131	.0110	.0012	.0088	.0063	.0030	.0003	.0061	.0024	.0007	.0000
4	.0009	.0012	.0015	.0012	.0007	.0005	.0003	.0000	.0003	.0001	.0000	.0000
5	.1540	.0402	.0081	.0002	.1855	.0597	.0160	.0020	.1855	.0668	.0187	.0021
6	.0365	.0243	.0062	.0001	.0586	.0343	.0114	.0014	.0576	.0298	.0103	.0012
7	.0168	.0094	.0031	.0001	.0162	.0113	.0067	.0012	.0157	.0091	.0035	.0003
8	.0026	.0018	.0006	.0000	.0024	.0018	.0011	.0007	.0021	.0011	.0005	.0001
9	.1241	.0297	.0052	.0001	.1879	.0591	.0154	.0020	.3302	.1076	.0290	.0034
10	.0474	.0132	.0024	.0000	.0703	.0308	.0093	.0010	.1068	.0980	.0358	.0043
11	.0141	.0038	.0006	.0000	.0200	.0107	.0036	.0003	.0297	.0344	.0295	.0047
12	.0016	.0003	.0000	.0000	.0023	.0014	.0004	.0000	.0036	.0047	.0052	.0055

Loading station	H_{h_1}	H_{h_2}	H_{α}	Mass of numbered segments (indicated by dashed lines in fig. 3), lb-sec^2/in.
1	0.76920	-0.24290	0.94927	1.36140×10^{-4}
2	.26915	.36389	.68317	5.12850
3	.07120	.19783	.26757	11.23601
4	.00603	.02576	.03167	19.79093
5	.83933	-.54309	.30095	1.65725
6	.34510	.13843	.21934	6.53497
7	.11126	.11783	.11109	14.61554
8	.01718	.02468	.02670	26.03627
9	1.00000	-1.00000	-.74970	1.02280
10	.49948	.24454	-1.00000	3.52098
11	.18076	.33132	-.57491	7.37383
12	.02502	.06876	-.10692	12.65363
$f_{calc.}$, cps . . .	51.1	114.0	91.1	
$f_{exp.}$, cps . . .	52.0	115.0	87.0	

TABLE I.- STRUCTURAL INFLUENCE COEFFICIENTS AND RELATED INFORMATION

AS INDICATED IN FIGURE 3 - Continued

(i) Wing 15

Loading station	Deflections for a 10-lb load, in inches, at loading station -											
	1	2	3	4	5	6	7	8	9	10	11	12
1	0.4285	0.1155	0.0140	0.0000	0.4655	0.1735	0.0432	0.0040	0.4585	0.2050	0.0635	0.0085
2	.1167	.0771	.0156	.0004	.1156	.0737	.0267	.0033	.1095	.0650	.0266	.0038
3	.0156	.0151	.0126	.0010	.0141	.0112	.0071	.0017	.0076	.0050	.0023	.0002
4	.0000	.0003	.0008	.0013	.0000	.0000	.0000	.0001	.0000	.0000	.0000	.0000
5	.4610	.1155	.0135	.0000	.5285	.1865	.0445	.0040	.5720	.2405	.0755	.0100
6	.1725	.0760	.0115	.0000	.1896	.1077	.0302	.0030	.1873	.1169	.0484	.0069
7	.0426	.0269	.0072	.0000	.0449	.0293	.0142	.0020	.0439	.0306	.0151	.0028
8	.0028	.0026	.0016	.0001	.0025	.0021	.0015	.0007	.0008	.0011	.0008	.0001
9	.4645	.1080	.0110	.0000	.5770	.1910	.0440	.0035	.7200	.2860	.0890	.0120
10	.2050	.0645	.0070	.0000	.2455	.1145	.0310	.0020	.2655	.1830	.0650	.0095
11	.0661	.0277	.0032	.0001	.0830	.0490	.0158	.0013	.0897	.0700	.0470	.0082
12	.0084	.0035	.0002	.0000	.0102	.0064	.0028	.0003	.0095	.0087	.0076	.0044

Loading station	H_{h_1}	H_{h_2}	H_{α}	Mass of numbered segments (indicated by dashed lines in fig. 3), lb-sec^2/in.
1	0.7953	-0.3994	0.9952	1.3158×10^{-4}
2	.2578	.4370	.6154	4.5767
3	.0344	.1462	.3366	9.6389
4	.0002	.0040	.0137	16.7288
5	.9017	-.6596	.6167	1.4751
6	.3918	.3605	-.0118	5.5663
7	.1055	.2157	.0689	12.1104
8	.0063	.0291	.0446	21.3516
9	1.0000	-1.0000	-.2257	1.0365
10	.4923	.1594	-1.0000	3.3430
11	.1926	.3239	-.7010	6.7124
12	.0249	.0591	-.1485	11.3430
$f_{calc.}$, cps . . .	28.2	73.8	95.3	
$f_{exp.}$, cps . . .	24.0	67.0	81.0	

TABLE I.- STRUCTURAL INFLUENCE COEFFICIENTS AND RELATED INFORMATION

AS INDICATED IN FIGURE 3 - Concluded

(j) Magnesium flat plate

Loading station	Deflections for a 6-lb load, in inches, at loading station -											
	1	2	3	4	5	6	7	8	9	10	11	12
1	0.4670	0.2034	0.0447	0.0040	0.4794	0.2598	0.0976	0.0148	0.4768	0.2732	0.1256	0.0278
2	.2049	.1505	.0539	.0057	.1915	.1371	.0728	.0154	.1780	.1155	.0598	.0150
3	.0480	.0519	.0350	.0067	.0440	.0391	.0290	.0098	.0350	.0241	.0135	.0035
4	.0035	.0046	.0063	.0049	.0010	.0019	.0022	.0012	.0012	.0007	.0006	.0002
5	.4754	.1926	.0464	.0032	.5088	.2569	.0962	.0136	.5152	.2996	.1360	.0294
6	.2555	.1371	.0410	.0322	.2513	.1594	.0690	.0124	.2524	.1586	.0798	.0186
7	.0943	.0704	.0288	.0028	.0969	.0700	.0438	.0092	.0859	.0587	.0333	.0092
8	.0139	.0131	.0089	.0013	.0098	.0117	.0084	.0047	.0068	.0048	.0034	.0011
9	.4894	.1864	.0416	.0028	.5248	.2578	.0896	.0116	.5512	.3168	.1420	.0302
10	.2784	.1152	.0259	.0017	.2951	.1596	.0595	.0083	.3126	.2027	.0985	.0207
11	.1236	.0571	.0136	.0009	.1332	.0805	.0352	.0046	.1430	.1014	.0589	.0148
12	.0260	.0138	.0030	.0002	.0256	.0175	.0087	.0014	.0252	.0193	.0127	.0065

Loading station	H_{h_1}	H_{h_2}	H_{α}	Mass of numbered segments (indicated by dashed lines in fig. 3), lb-sec^2/in.
1	0.9513	-0.2900	0.0328	1.4378×10^{-4}
2	.4424	1.0000	.0829	3.6957
3	.1171	.6900	.1339	5.9536
4	.0071	.1045	.0242	8.3239
5	.9135	-.4063	1.0000	1.5503
6	.5398	.3595	-.0902	3.8082
7	.2257	.5305	.0189	6.0661
8	.0297	.2037	.0352	8.3239
9	1.0000	-.9724	-.1673	1.4941
10	.6005	-.4752	-.3745	3.7520
11	.2923	-.1451	-.3447	6.0098
12	.0598	.0192	-.0794	8.3239
$f_{calc.}$, cps . . .	19.0	54.6	75.7	
$f_{exp.}$, cps . . .	19.5	60.0	104.0	

TABLE II.- WING PARAMETERS

Wing	Type[a]	Λ	l, in.	A	x_1, percent chord	x_o, percent chord	a	$a + x_\alpha$	r_α^2	$\mu_{s,r}$	f_{h_1}, cps	f_{h_2}, cps	f_α, cps
1	A	60°	19.31	2.14	46.8	40	-0.200	-0.064	0.2569	5.91	29.8	88	78
2	A	60°	19.31	2.14	44.6	40	-.200	-.108	.2478	5.70	30	94	81
3	B	60°	19.31	2.14	44.6	40	-.200	-.108	.2293	5.80	51.8	148	113
4	C	60°	19.31	2.14	45	40	-.200	-.100	.2431	6.98	36	100	128
5	C	60°	19.31	2.14	45	40	-.200	-.100	.2368	5.85	36	105	131
6	C	60°	19.31	2.14	45	40	-.200	-.100	.2402	6.52	40	110	140
7	C	60°	19.31	2.14	45	40	-.200	-.100	.2581	5.41	39.2	104	139
8	C	60°	19.31	2.14	45	40	-.200	-.100	.3040	5.85	42	111	148
9	C	60°	19.31	2.14	45.4	40	-.200	-.092	.3022	6.11	45	112	147
10	F	60°	17.00	2.14	50	50	0	0	.3213	7.15	19.5	104	60
11	D	45°	32.75	3.84	45.5	40	-.200	-.090	.2354	14.10	45.5	108	90
12	E	45°	32.75	3.84	46.5	40	-.200	-.070	.2443	11.08	21	58	81
13	D	53°8'	24.56	2.64	46	40	-.200	-.080	.1961	11.45	55	126	99
14	D	53°8'	24.56	2.64	46	40	-.200	-.080	.1952	10.83	52	115	87
15	E	53°8'	24.56	2.64	46.8	40	-.200	-.064	.2427	9.12	53	64.5	78

[a]See figure 1.

TABLE III.- MODE SHAPE AND SPANWISE VARIATION OF x_1, r_α^2, and μ_s

Station	Fraction of span	H_{h_1}	H_α	x_1, percent chord	r_α^2	μ_s	H_{h_1}	H_α	x_1, percent chord	r_α^2	μ_s
		Wing 4					Wing 5				
0	0	0	0	44.9	0.2431	6.98	0	0	44.9	0.2368	5.85
1	.1111	.0039	.0305	44.9	.2453	6.99	.0039	.0305	44.9	.2405	5.88
2	.2222	.0297	.1186	44.9	.2488	7.00	.0297	.1186	44.9	.2442	5.88
3	.3333	.0695	.2526	44.8	.2532	7.01	.0695	.2526	44.8	.2482	5.89
4	.4444	.1289	.4189	44.8	.2580	7.04	.1289	.4189	44.8	.2562	5.92
5	.5555	.2164	.5951	44.7	.2669	7.1	.2164	.5951	44.7	.2660	5.97
6	.6667	.3383	.7369	44.6	.2793	7.18	.3383	.7369	44.6	.2810	6.04
7	.7778	.5023	.8315	45.0	.3045	7.52	.5023	.8315	45.0	.3060	6.36
8	.8889	.7266	.9286	45.4	.3457	8.63	.7266	.9286	45.4	.3535	7.26
9	1.0000	1.0000	1.0000	50.2	.6036	19.90	1.0000	1.0000	50.2	.5860	16.75
		Wing 7					Wing 8				
0	0	0	0	45.1	0.2582	5.41	0	0	45.2	0.3040	5.85
1	.1111	.0064	.0461	45.1	.2630	5.50	.0038	.0191	45.3	.3122	5.95
2	.2222	.0208	.1135	45.1	.2704	5.57	.0199	.1053	45.4	.3189	6.00
3	.3333	.0496	.1879	45.1	.2801	5.65	.0519	.2632	45.4	.3344	6.10
4	.4444	.1000	.2908	45.1	.2943	5.75	.1069	.4976	44.2	.3169	5.92
5	.5555	.1968	.4468	45.1	.2651	5.51	.1870	.7321	44.8	.3340	6.12
6	.6667	.3400	.6560	45.0	.2803	5.65	.3015	.8804	45.5	.3592	6.37
7	.7778	.5200	.8227	44.9	.3096	5.98	.4626	.9474	45.2	.3315	6.3
8	.8889	.7320	.9433	45.6	.3690	6.54	.6855	.9809	45.6	.3741	7.2
9	1.0000	1.0000	1.0000	50.4	.6045	10.75	1.0000	1.0000	50.4	.6117	8.55
		Wing 9					Wing 10				
0	0	0	0	45.3	0.3022	6.11	0	0	50.0	0.3213	7.15
1	.1111	.0038	.0191	45.3	.3097	6.32	.0165	.0212	↓	.3200	7.98
2	.2222	.0199	.1053	45.4	.3192	6.37	.0662	.1217		.3183	9.03
3	.3333	.0519	.2632	45.4	.3309	6.47	.1390	.2751		.3162	10.40
4	.4444	.1069	.4976	45.3	.3141	6.28	.2357	.4921		.3233	12.25
5	.5555	.1870	.7321	45.4	.3304	6.50	.3515	.7513		.3093	14.91
6	.6667	.3015	.8804	45.4	.3526	6.76	.4880	.8889		.3034	19.03
7	.7778	.4626	.9474	45.2	.3283	6.68	.6427	.9524		.2940	26.27
8	.8889	.6855	.9809	45.6	.3627	7.64	.8172	.9894		.2223	42.27
9	1.0000	1.0000	1.0000	50.2	.6486	9.06	1.0000	1.0000		.1765	93.55
		Wing 12					Wing 13				
0	0	0	0	45.8	0.2443	11.08	0	0	45.5	0.1961	11.45
1	.1111	.0114	.0356	46.0	.2464	11.15	.0043	.0090	45.6	.1946	11.60
2	.2222	.0364	.1022	46.1	.2488	11.22	.0232	.0396	45.6	.1923	11.83
3	.3333	.0750	.2267	46.1	.2316	11.45	.0498	.0811	45.7	.1896	12.10
4	.4444	.1333	.4356	46.3	.2331	11.85	.1202	.1315	45.8	.1862	12.46
5	.5555	.2303	.6667	46.5	.2352	12.42	.2283	.1982	46.0	.1815	12.95
6	.6667	.3667	.8533	46.8	.2381	13.31	.3991	.3027	46.2	.1749	13.60
7	.7778	.5326	.9422	47.1	.2046	14.66	.5665	.5009	46.6	.1655	14.78
8	.8889	.7439	.9867	47.7	.2022	18.35	.7725	.7423	47.2	.1495	18.00
9	1.0000	1.0000	1.0000	49.0	.1838	50.00	1.0000	1.0000	48.3	.1175	29.50
		Wing 14					Wing 15				
0	0	0	0	45.5	0.1952	10.83	0	0	46.0	0.2427	9.12
1	.1111	.0043	.0090	45.6	.1931	11.00	.0040	.0177	46.1	.2545	9.35
2	.2222	.0232	.0396	45.7	.1910	11.15	.0264	.0735	46.2	.2567	9.55
3	.3333	.0498	.0811	45.8	.1883	11.43	.0600	.1559	46.2	.2401	9.81
4	.4444	.1202	.1315	45.9	.1846	11.82	.1240	.2325	46.4	.2412	10.13
5	.5555	.2283	.1982	46.1	.1797	12.33	.2240	.3912	46.6	.2428	10.70
6	.6667	.3991	.3027	46.3	.1731	12.91	.3664	.5382	46.9	.2452	11.71
7	.7778	.5665	.5009	46.6	.1631	14.20	.5384	.6912	47.1	.2118	13.45
8	.8889	.7725	.7423	47.3	.1477	17.50	.7440	.8471	47.7	.2075	17.00
9	1.0000	1.0000	1.0000	48.5	.1165	29.50	1.0000	1.0000	49.9	.2581	27.40

TABLE IV.- EXPERIMENTAL AND CALCULATED RESULTS

Wing	M_e	V_e, fps	f_z, cps	ρ_e, slugs/cu ft	q_e, lb/sq ft	$\mu_{e,r}$	V_R, fps	f_R, cps	$\frac{V_e}{V_R}$	$\frac{b\omega_R}{V_c}\sqrt{\mu}$	V_2, fps	$\frac{V_e}{V_2}$	$\frac{V_e}{V_2}\sqrt[4]{\frac{0.00238}{\rho_e}}$
1	0.857 1.001	901.1 1,068.0	49.4 89.6	0.000631 0.000980	255.9 558.9	22.3 14.35	743 640	69.6 71.6	1.210 1.670	3.21 2.54	----- -----	----- -----	----- -----
2	0.832	912.4	53.3	0.001572	654.2	8.63	-----	-----	-----	1.99	-----	-----	-----
3	0.794 895	852.0 980.6	145.0 120.0	0.001740 .001473	631.6 708.3	7.93 9.36	807 -----	125.8 -----	1.056 -----	2.71 3.23	----- 1,145	----- 0.856	----- 0.965
4	1.006	1,082.7	60.0	0.001348	789.8	12.32	1,196	119.4	0.905	3.83	1,240	0.874	1.006
5	0.711	770.2	-----	0.001826	541.5	7.62	1,080	133.0	0.713	3.05	1,007	0.765	0.817
6	0.853	942.0	67.4	0.001124	497.0	13.80	-----	-----	-----	4.30	1,410	0.668	0.810
7	0.970	1,050.3	81.2	0.001396	769.8	9.22	1,110	128.7	0.941	3.57	1,156	0.908	1.037
8	0.909	994.3	76.0	0.001057	522.2	13.16	1,383	141.3	0.718	5.19	903	1.100	1.275
9	0.777	865.6	76.2	0.001313	491.8	11.07	1,309	143.0	0.666	4.04	-----	-----	-----
10	0.400 .496 .600 .700 .800 .510 .590 .912	441.3 537.2 654.7 764.7 870.1 558.8 644.9 974.5	51.7 51.9 51.0 52.5 50.0 44.5 ------- 50.6	0.001154 .000928 .000742 .000756 .000501 .00207 .00153 .000691	112.4 133.9 159.1 221.0 189.7 323.0 318.5 328.0	14.75 18.33 22.91 22.50 33.97 8.22 11.12 24.61	----- 760 ----- 789 ----- 609 ----- -----	----- 39.1 ----- 35.5 ----- 46.4 ----- -----	----- 0.707 ----- .969 ----- .917 ----- -----	1.72 1.96 2.17 2.15 1.29 1.29 1.51 2.30	1,200 ----- ----- ----- ----- ----- 1,065 -----	0.368 ----- ----- ----- ----- ----- 0.606 -----	0.434 ----- ----- ----- ----- ----- 0.676 -----
11	0.707 .667 .692 .800 .624 .632 .889 .892 .807 .668	786.0 750.4 777.5 878.5 709.1 722.7 730.3 979.1 899.0 757.8	108.3 109.0 190.0 111.0 112.4 200.0 106.6 107.1 181.8 170/183	0.00173 .00176 .00172 .00063 .00178 .00177 .00039 .00080 .00126 .00171	534.5 494.6 520.8 244.0 447.0 462.0 102.7 385.0 508.0 492.1	19.35 19.01 19.45 53.12 18.80 18.90 85.80 41.82 26.55 19.58	Not discrete flutter points						
12	0.849	924.3	37.9	0.000787	336.1	33.52	992	52.3	0.932	3.93	1,057	0.875	1.157
13	0.516 .605 .710 .792 .865	583.0 670.0 772.7 850.1 930.5	160.4 144.5 134.5 122.0 116.6	0.001961 .001350 .000780 .000535 .000388	333.2 302.7 232.8 193.3 168.1	13.90 20.19 34.92 50.95 70.25	632 ----- 886 ----- 1,102	79.8 ----- 75.2 ----- 70.7	0.922 ----- .872 ----- .844	3.00 3.69 4.71 6.06 7.08	1,001 ----- ----- ----- 1,924	0.582 ----- ----- ----- .486	0.604 ----- ----- ----- .764
14	0.595 .746 .897	663.5 813.9 955.6	156.7 125.0 112.2	0.001685 .000705 .000341	156.7 233.4 155.7	15.30 36.60 75.65	548 ----- 975	75.3 ----- 65.7	1.210 ----- .977	----- ----- -----	----- ----- 2,010	----- ----- .485	----- ----- .790
15	0.858 .906	929.5 973.5	42.6 38.5	0.000640 .000484	276.4 229.3	33.90 44.82	905 971	52.2 54.7	1.027 1.001	3.84 4.43	1,384 -----	0.672 -----	0.963 -----

[redacted]

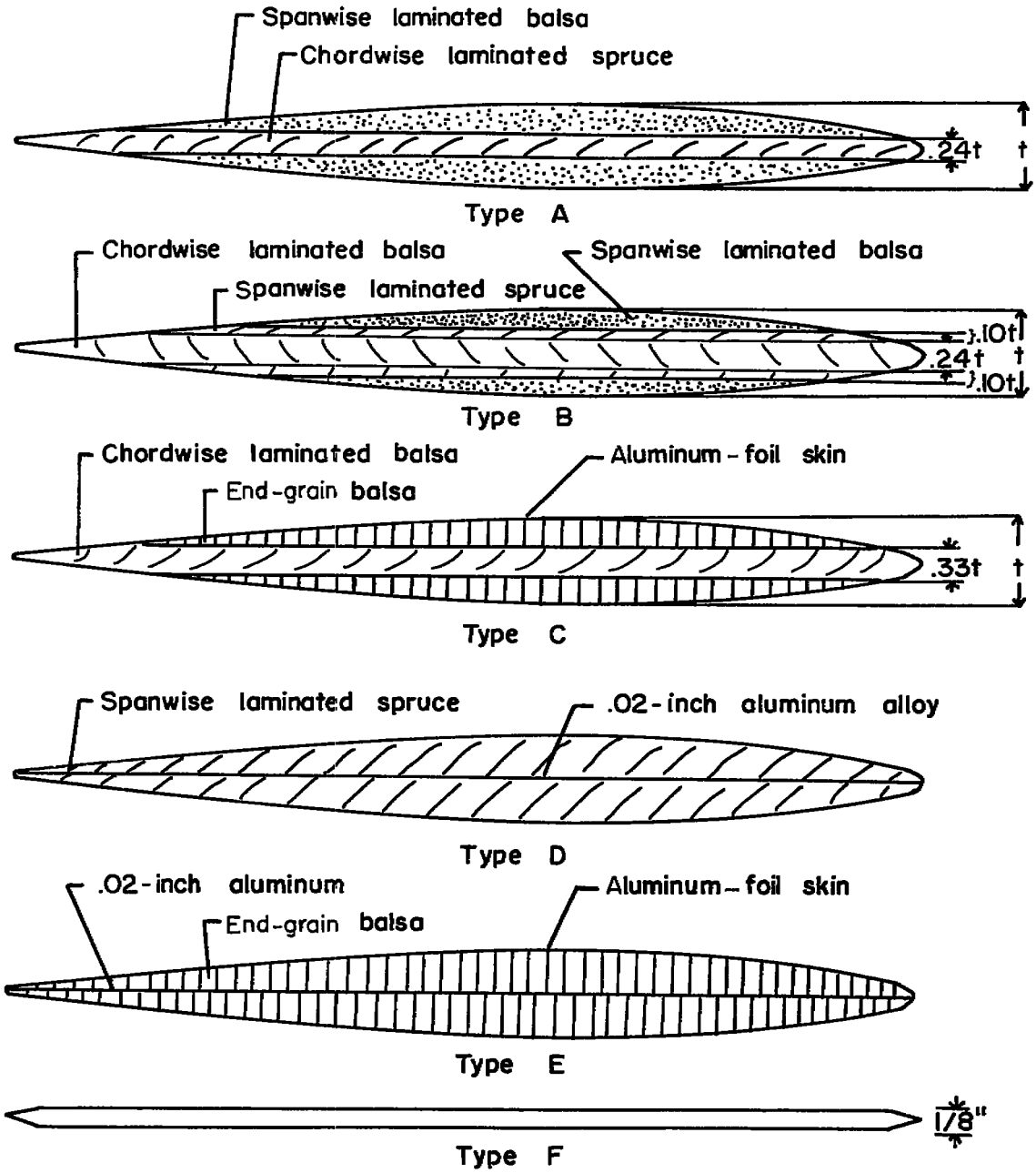

Figure 1.- Construction details of wings.

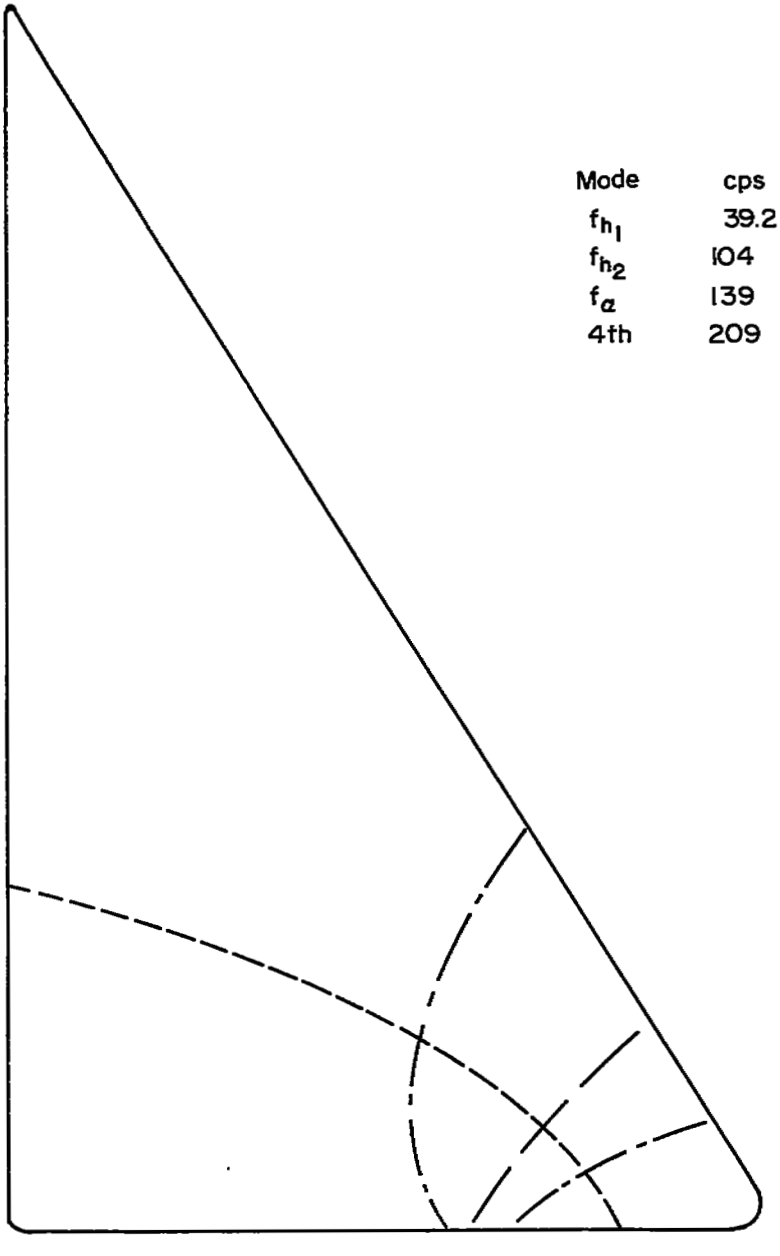

(a) 60° foil-covered wing (wings 4, 5, 6, 7, 8, and 9).

Figure 2.- Representative nodal patterns and frequencies of the various plan forms tested.

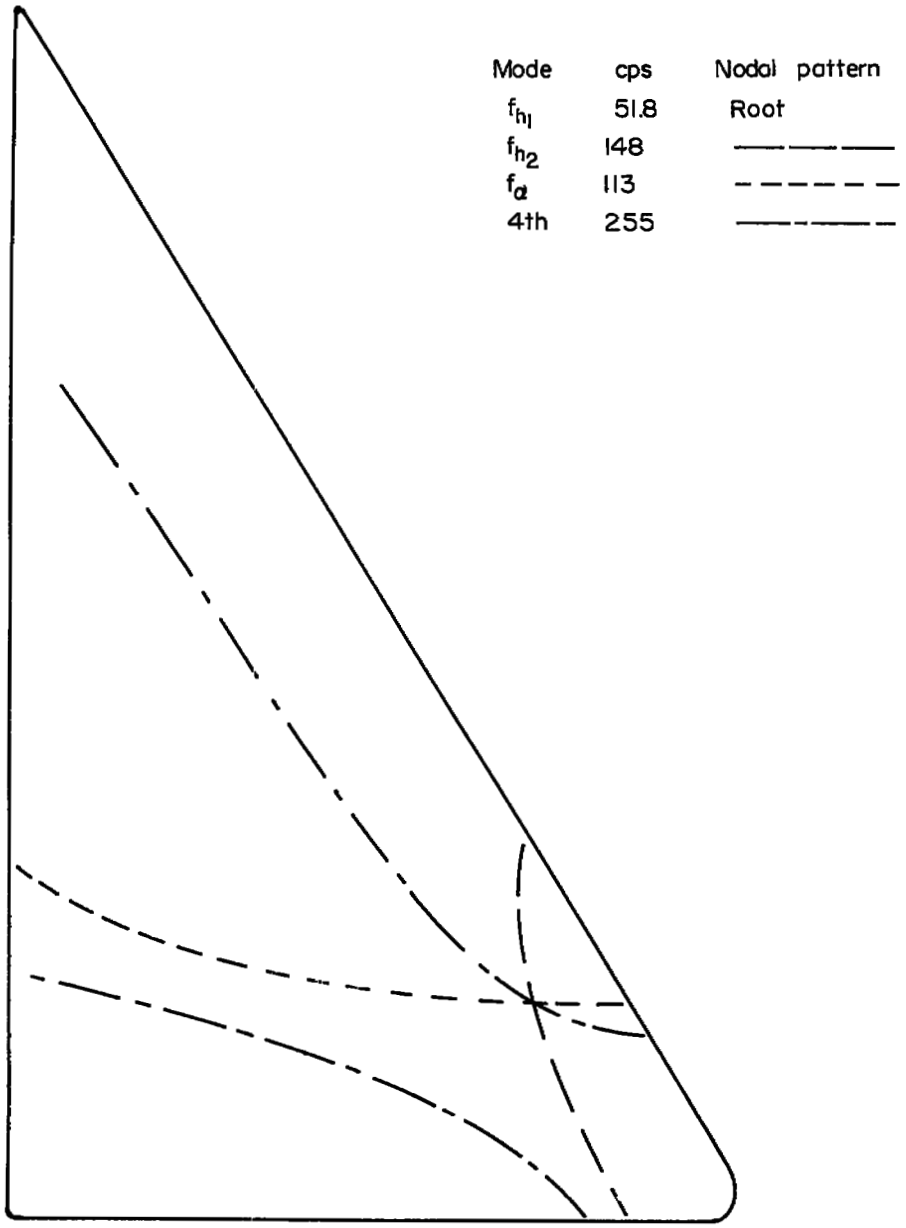

(b) 60° spruce and balsa wing (wings 1, 2, and 3).

Figure 2.- Continued.

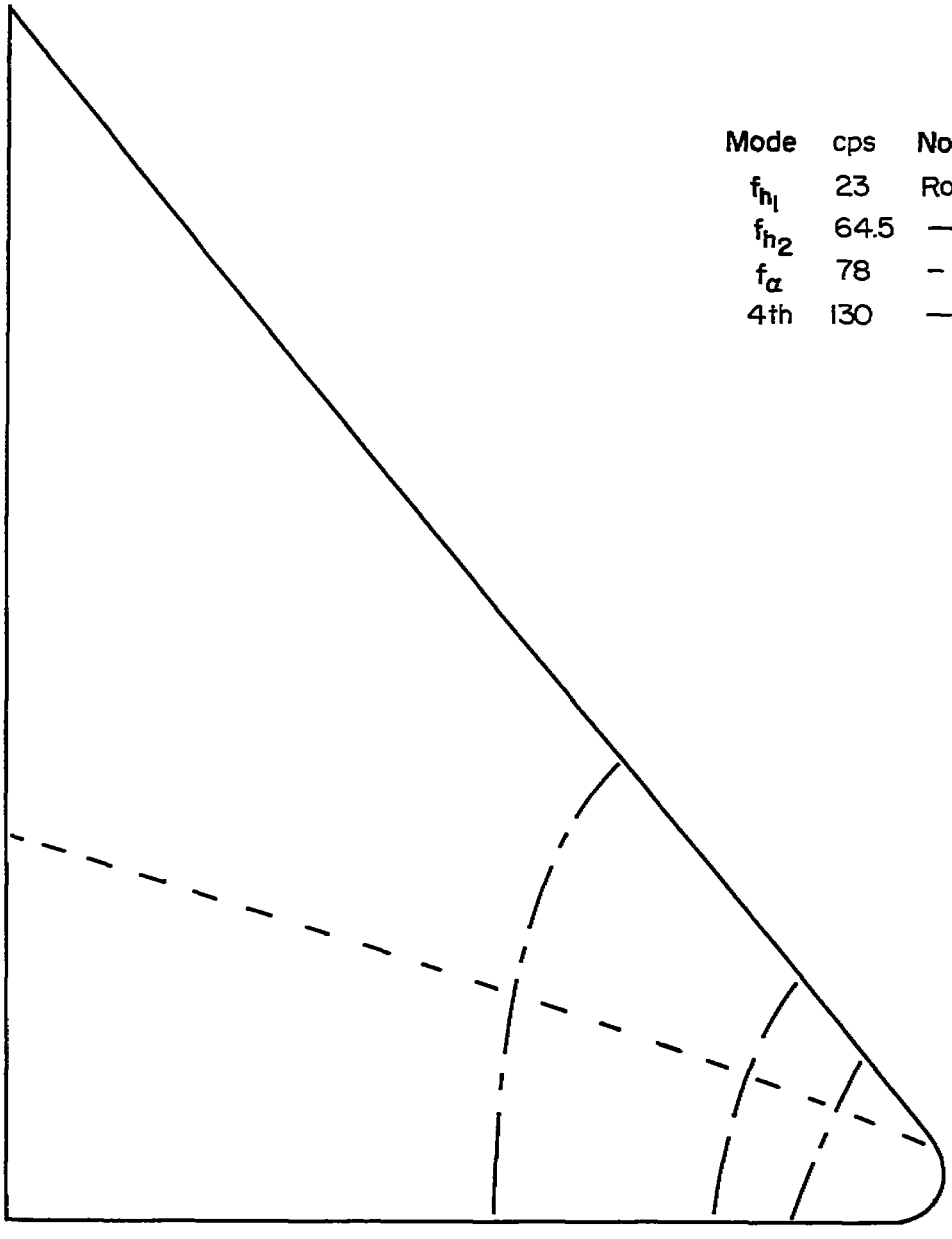

(c) 53° 8' foil-covered (wing 15).

Figure 2.- Continued.

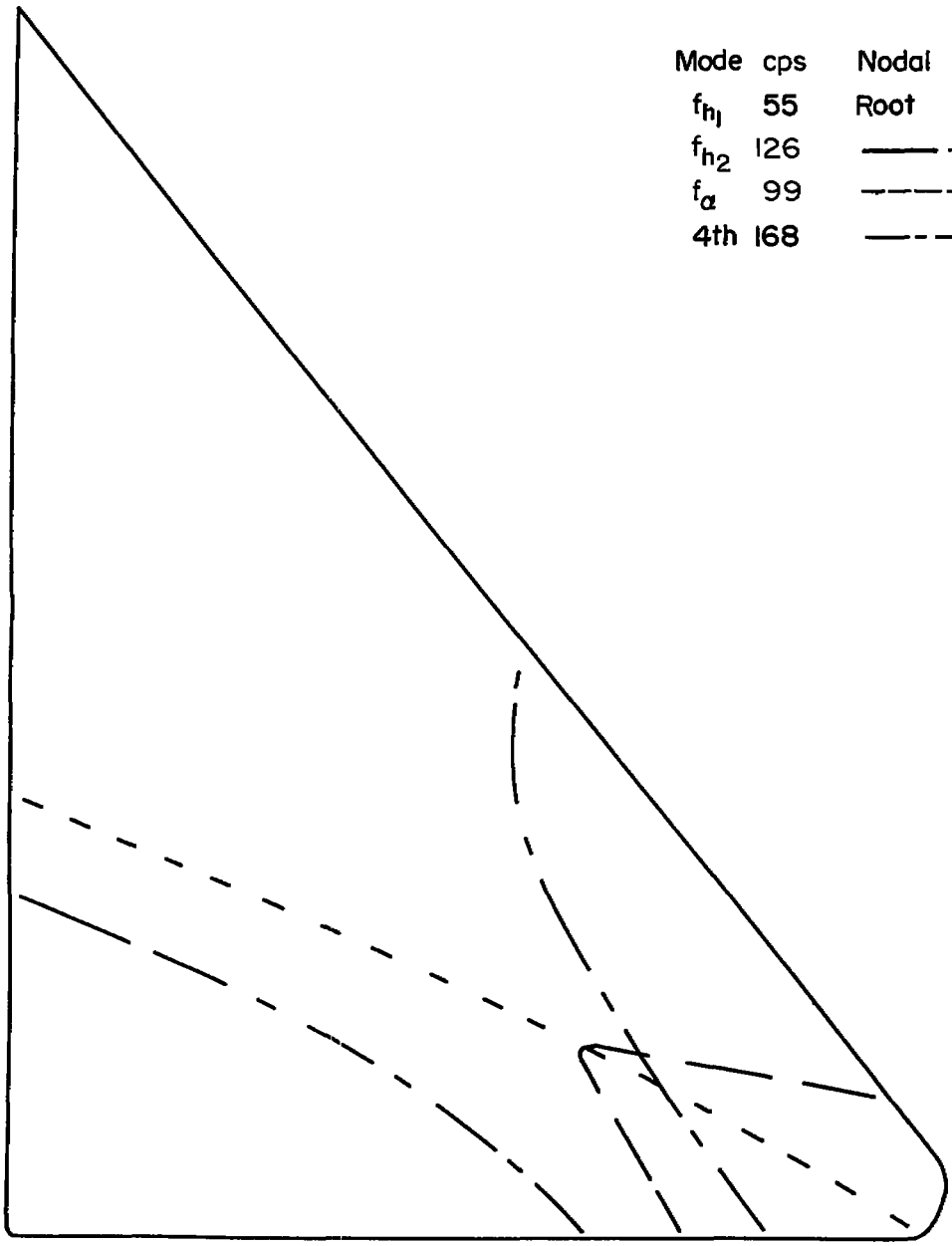

(d) 53° 8' spruce wing (wings 13 and 14).

Figure 2.- Continued.

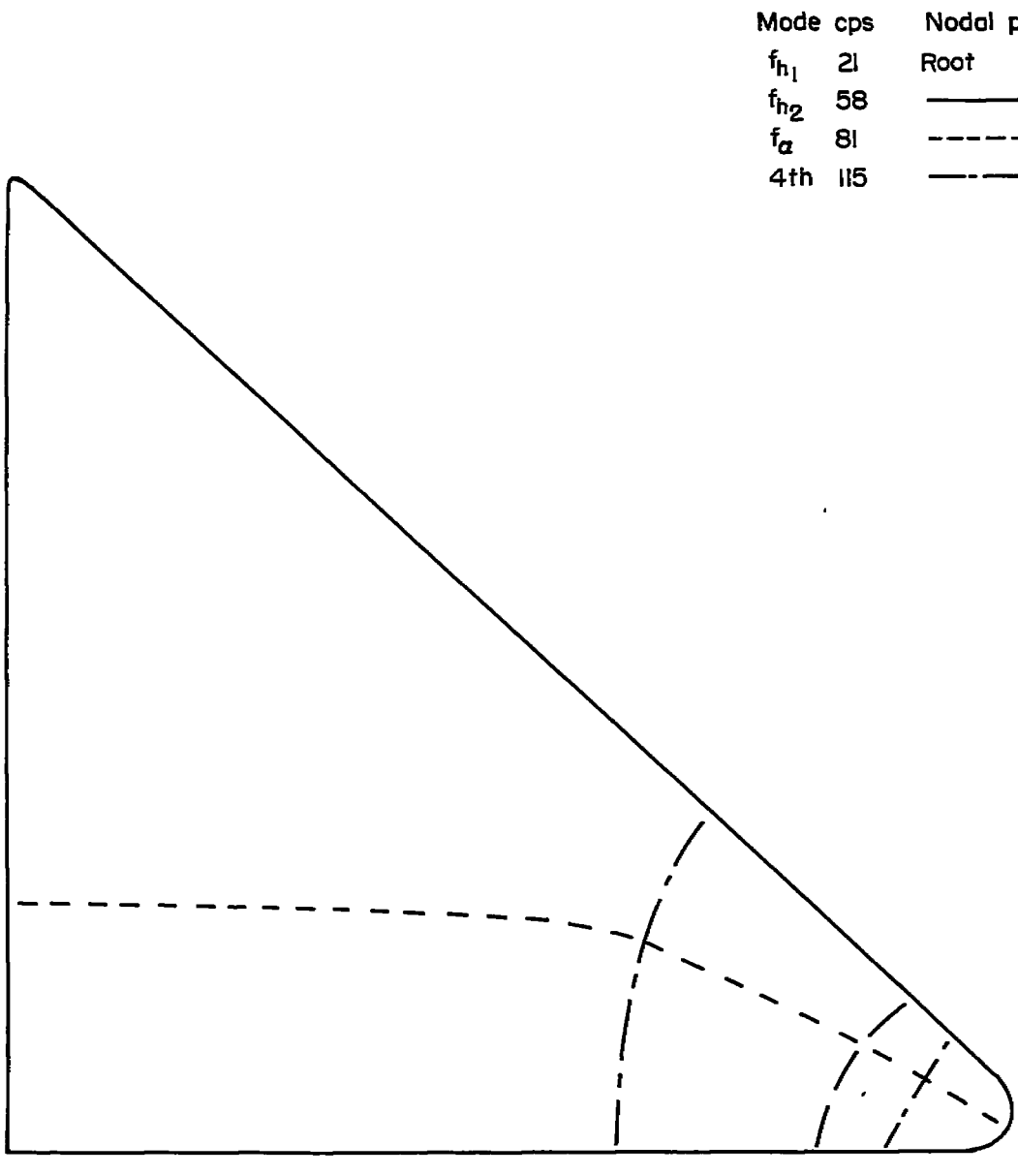

(e) 45° foil-covered wing (wing 12).

Figure 2.- Continued

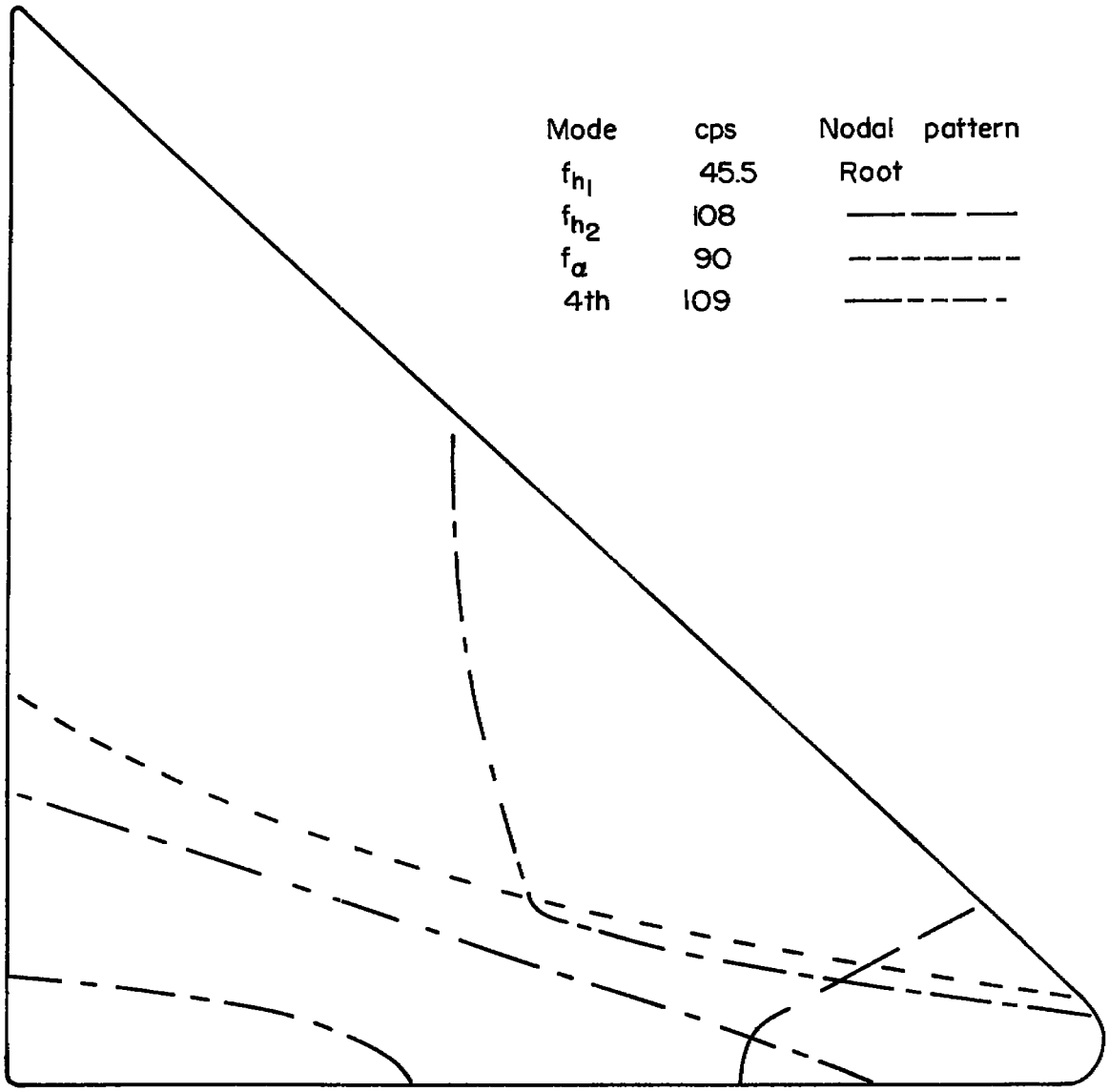

(f) 45° spruce wing (wing 11).

Figure 2.- Continued.

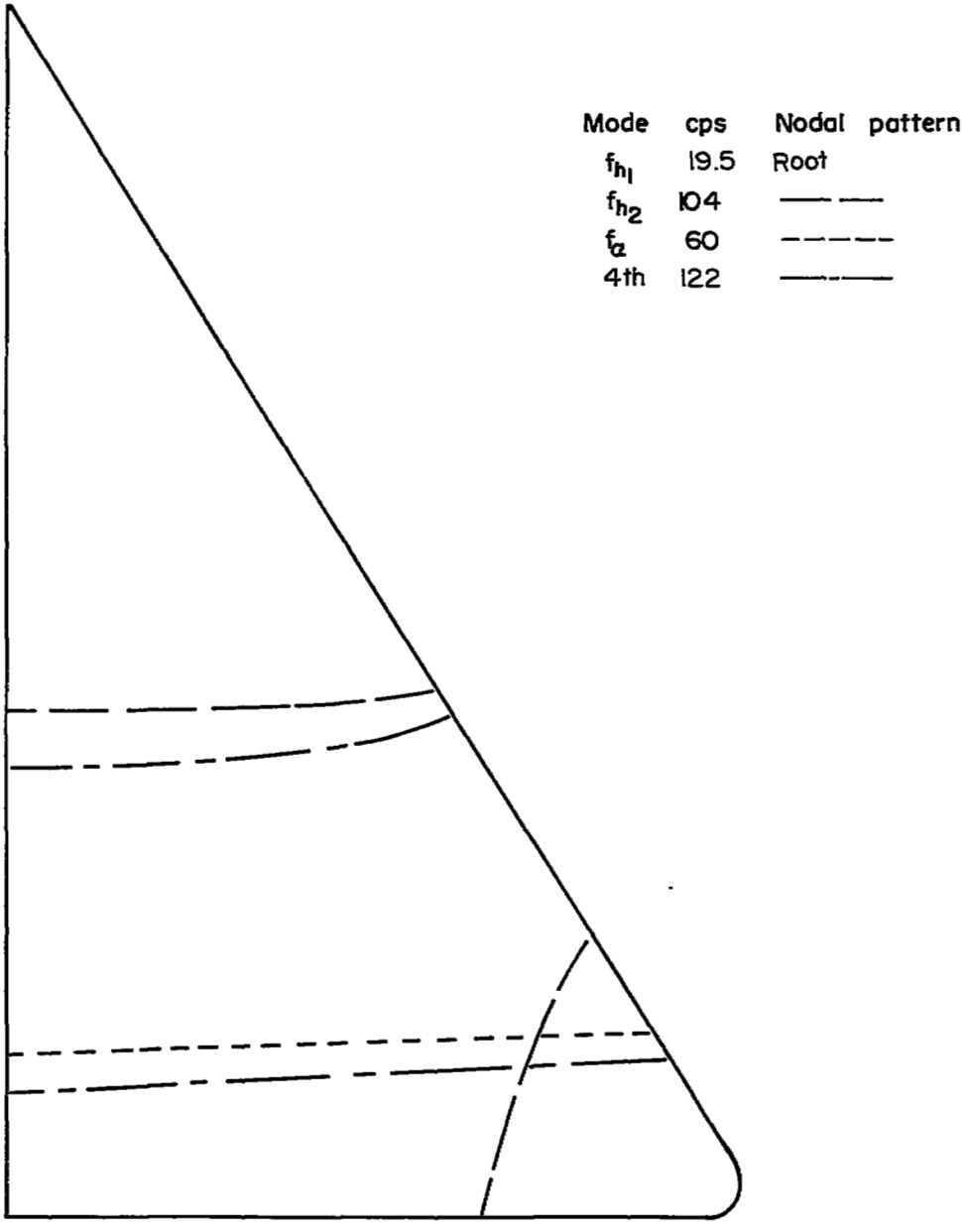

(g) 60° magnesium flat plate (wing 10).

Figure 2.- Concluded.

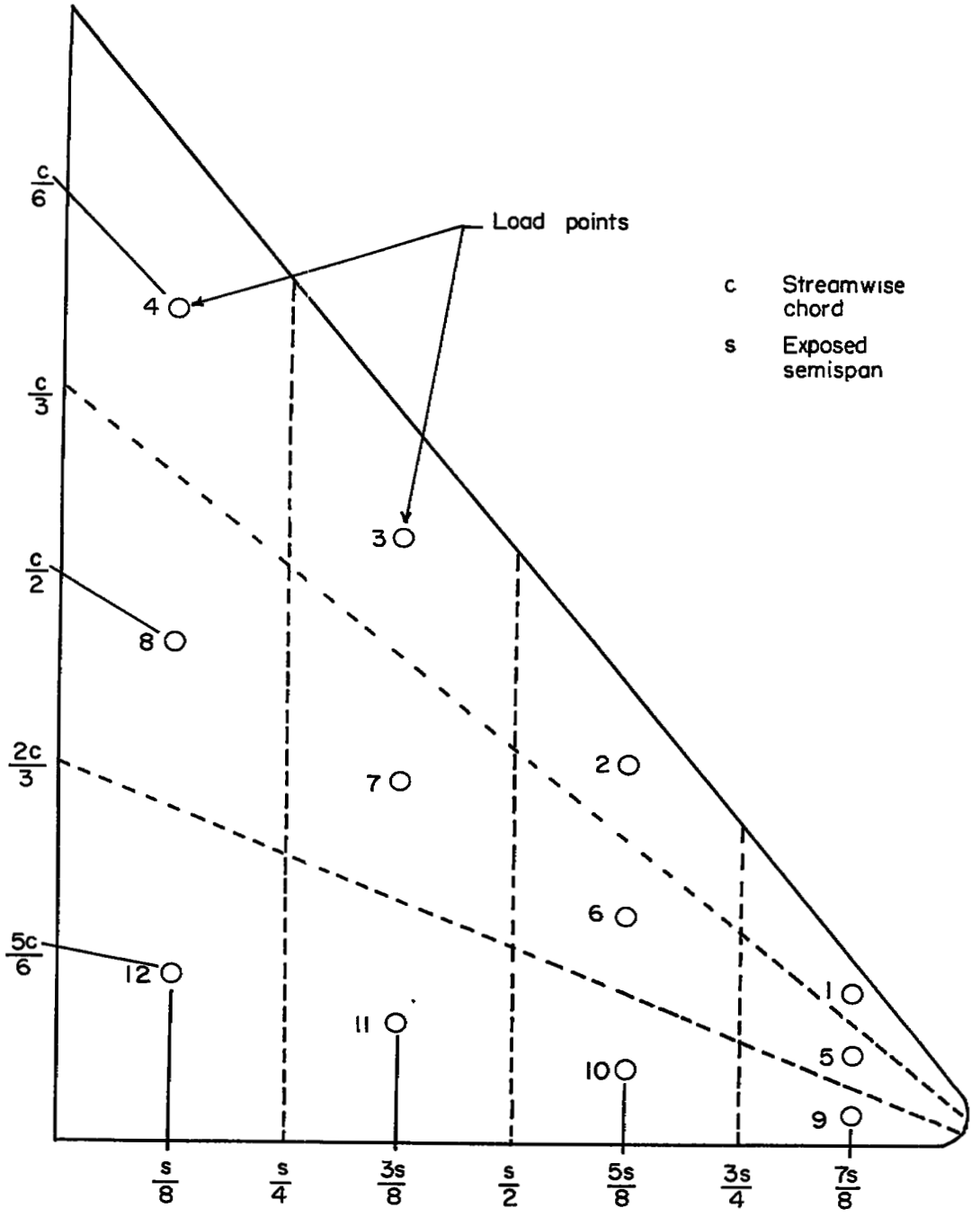

Figure 3.- Sketch of a delta plan form showing loading stations and mass segments. Typical of all wings tested.

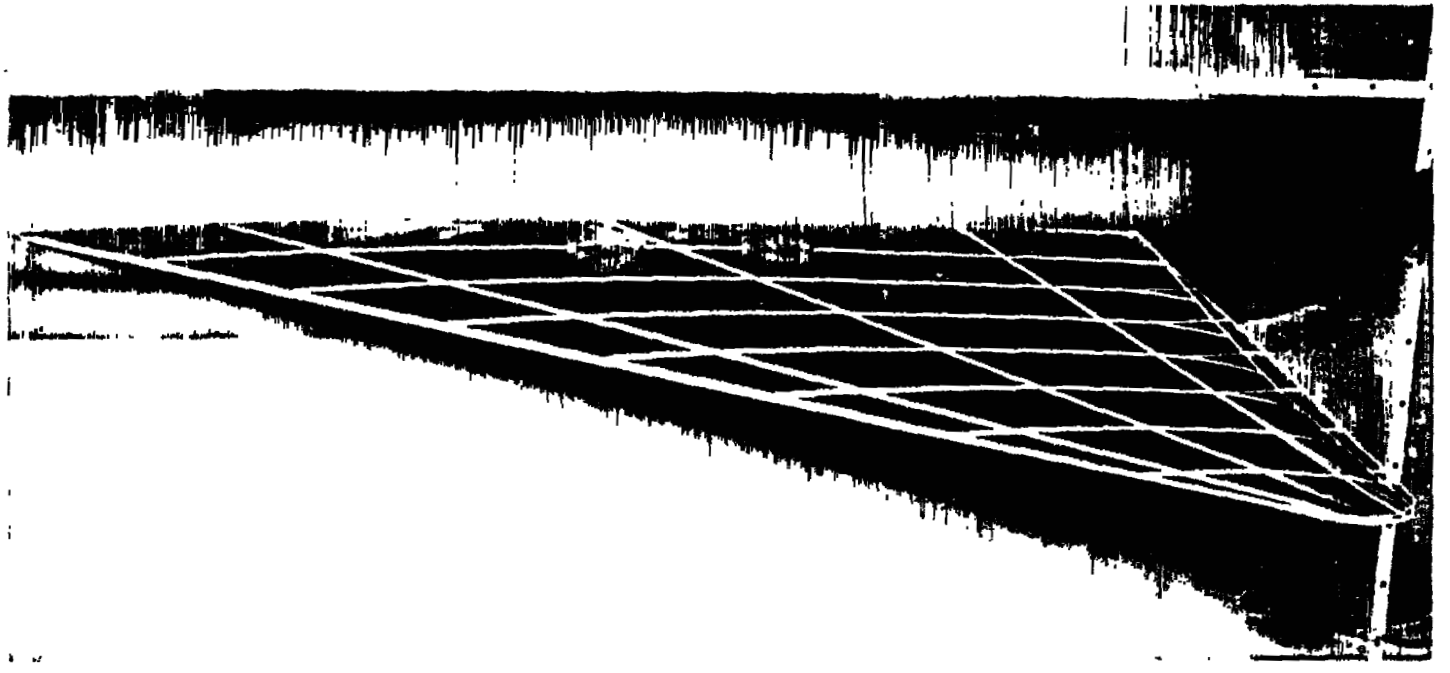

(a) Wing 1⅗. L-95889

Figure 4.- High-speed flash photographs showing flutter modes.

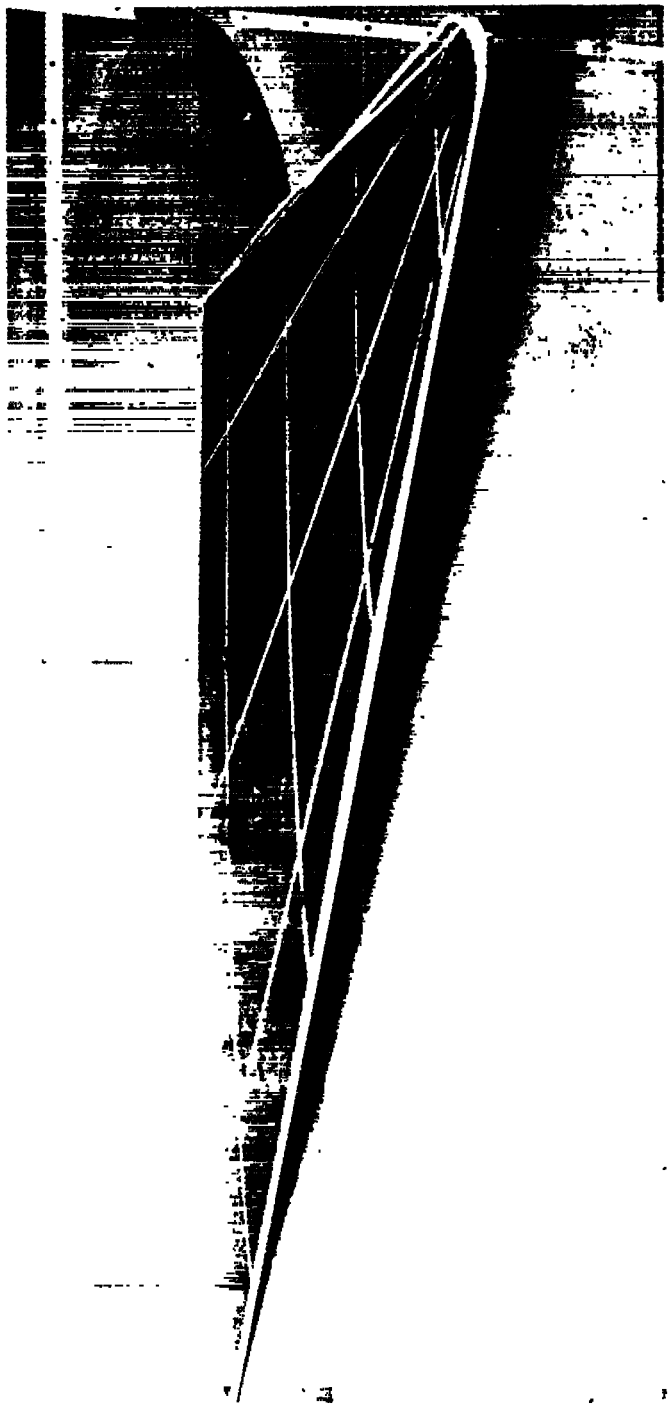

L-95890

(b) Wing 14.

Figure 4.- Concluded.

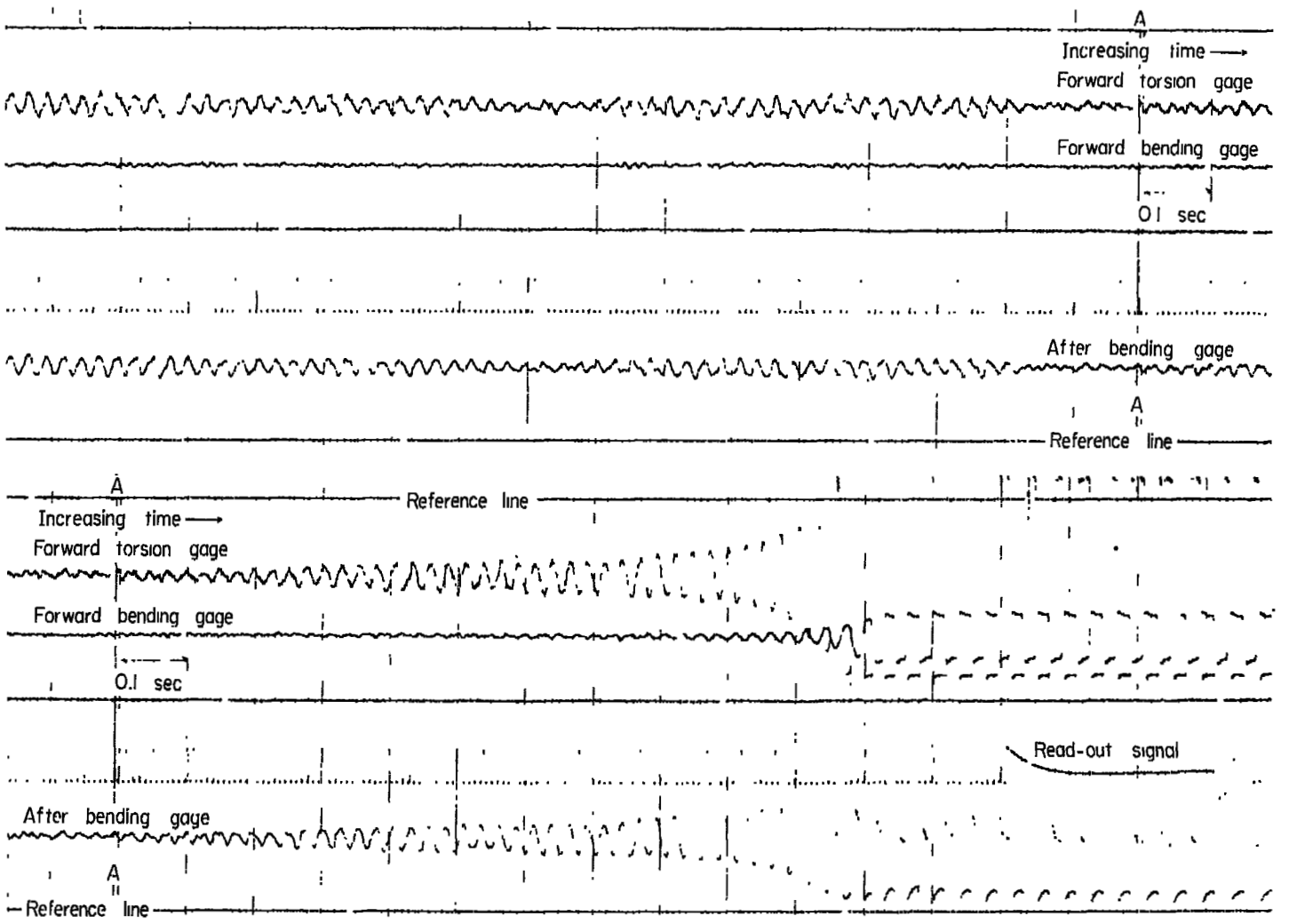

Figure 5.- Oscillograph record showing rapid buildup of flutter (wing 15).

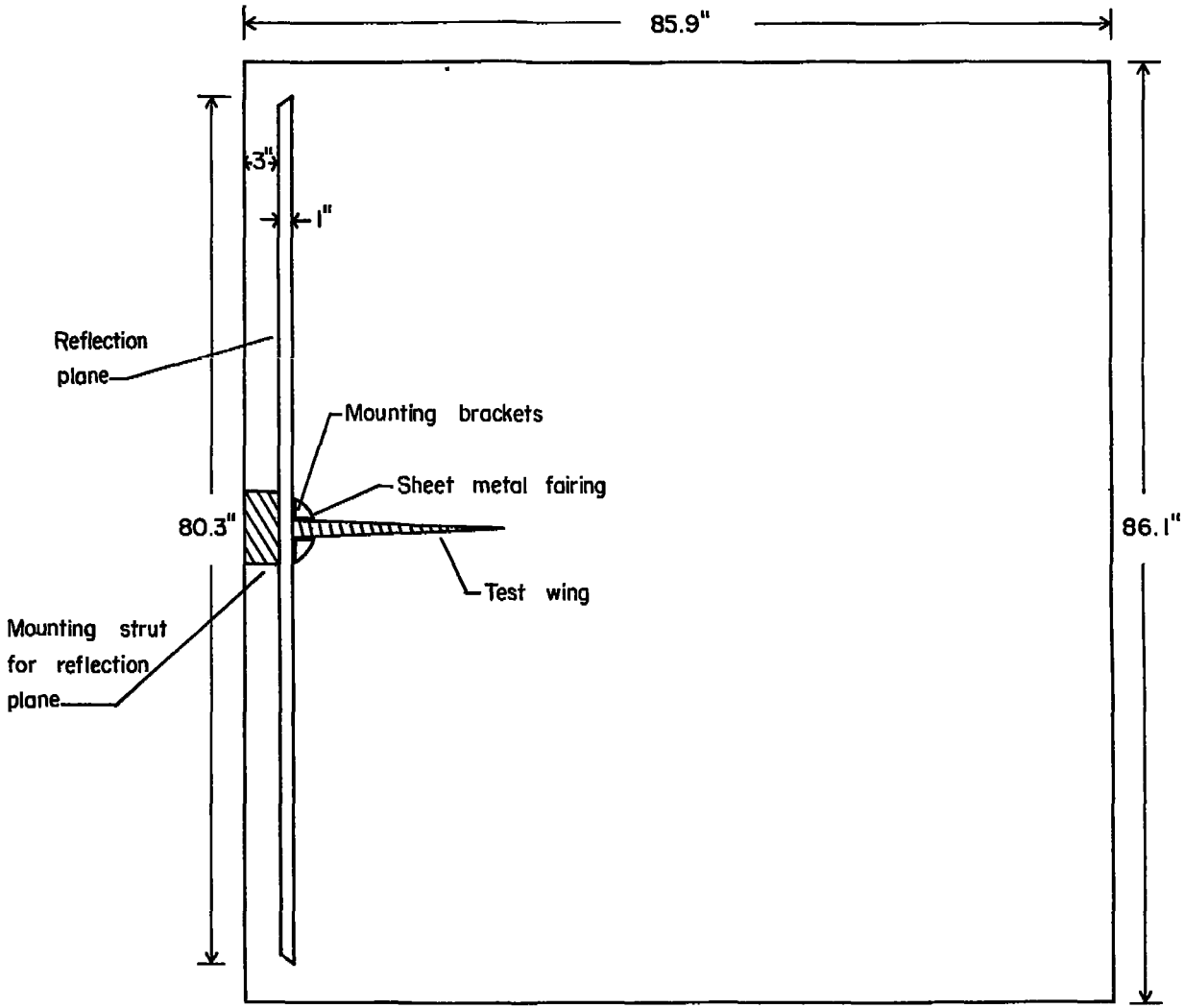

Figure 6.- Schematic section drawing of wing mounted in test section looking downstream.

L-88192.1

Figure 7.- Photograph of wing mounted on the reflection plane in the Langley 8-foot transonic pressure tunnel.

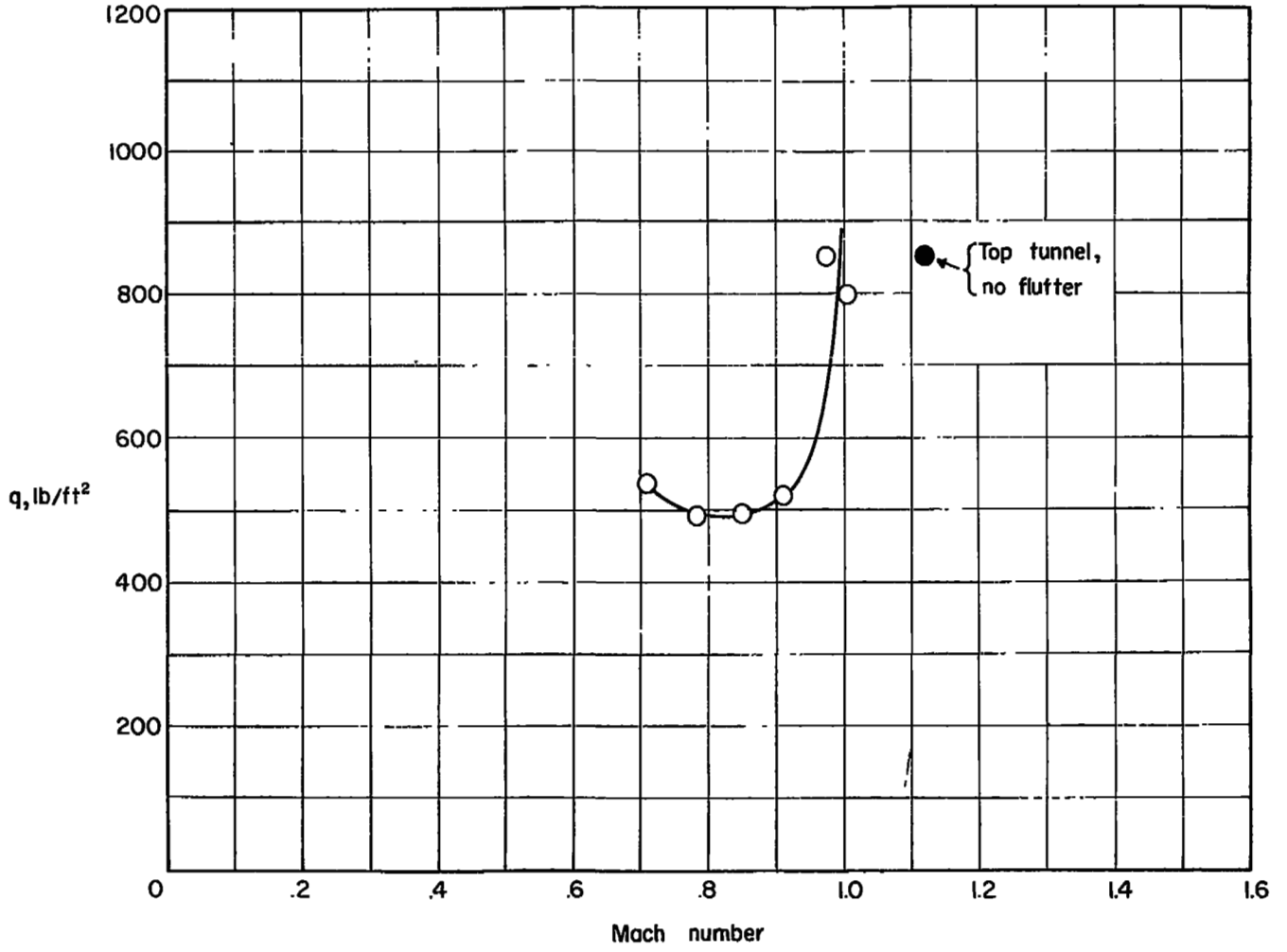

(a) 60° foil-covered wings.

Figure 8.- Effect of Mach number on the dynamic pressure at flutter.

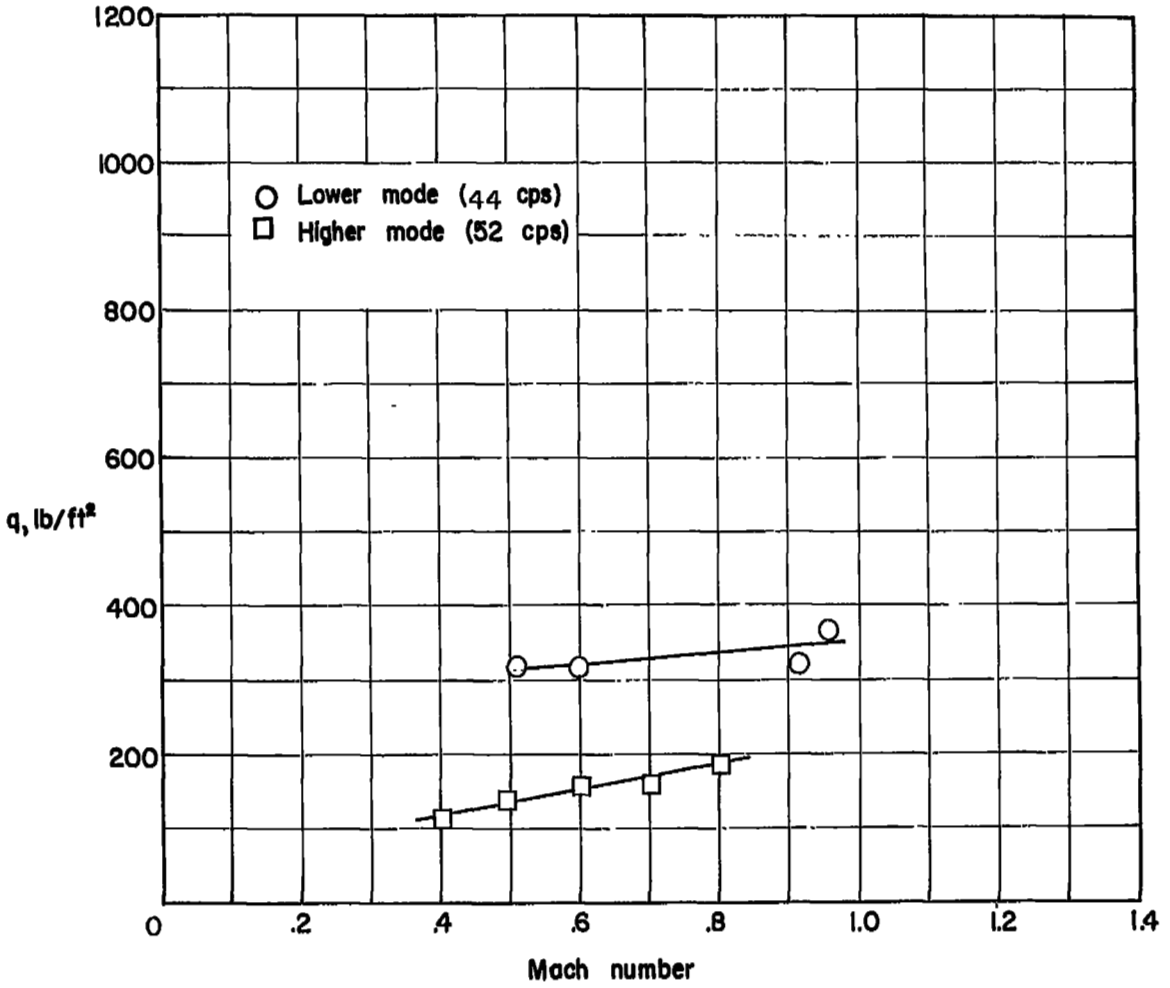

(b) 60° magnesium flat plate.

Figure 8.- Continued.

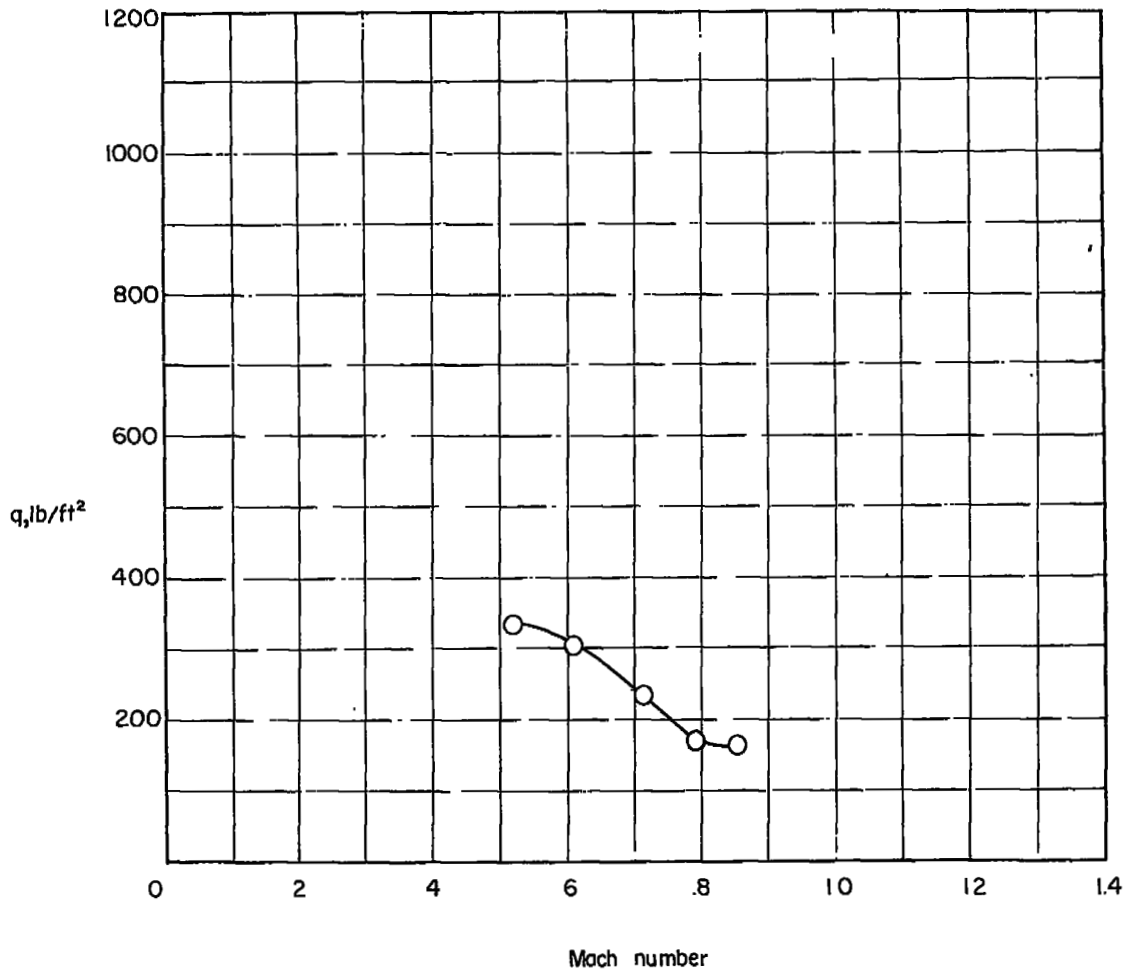

(c) 53° 8' spruce wing.

Figure 8.- Concluded.

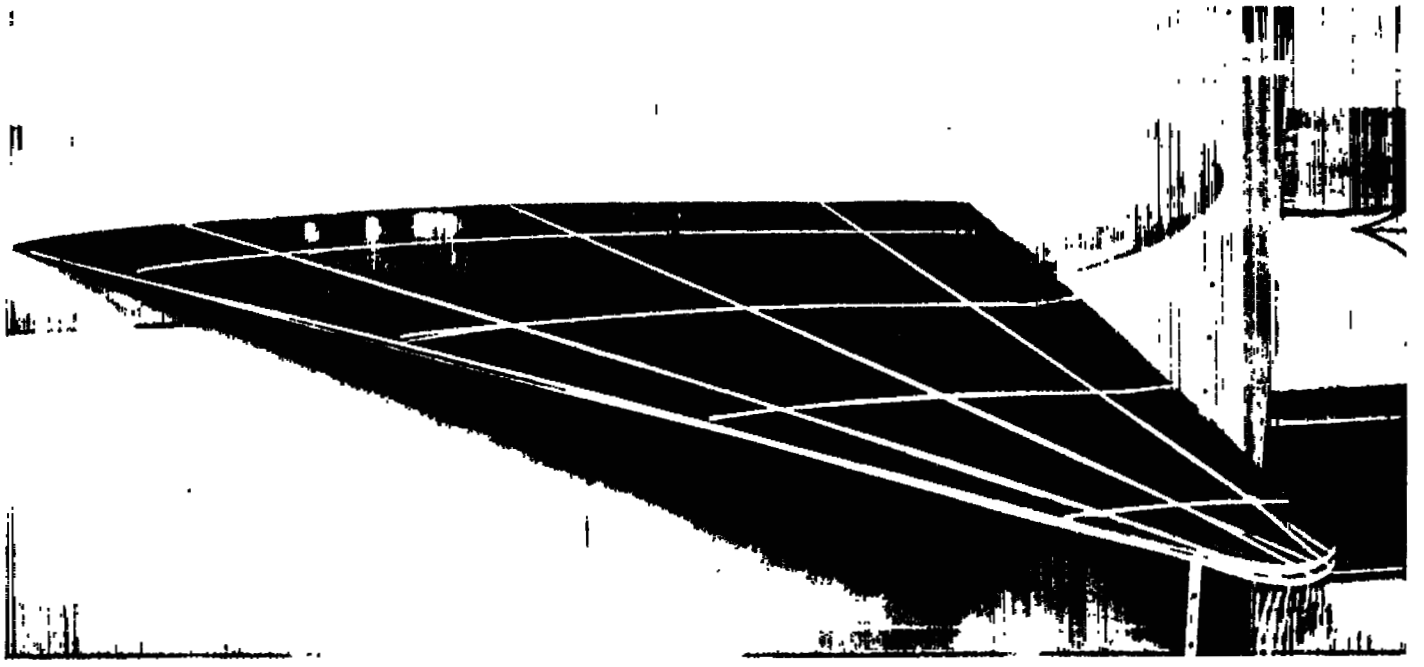

(a) Mach number, 0.633; frequency, 200 cps. L-95891

Figure 9.- High-speed flash photographs of 45° spruce wing.

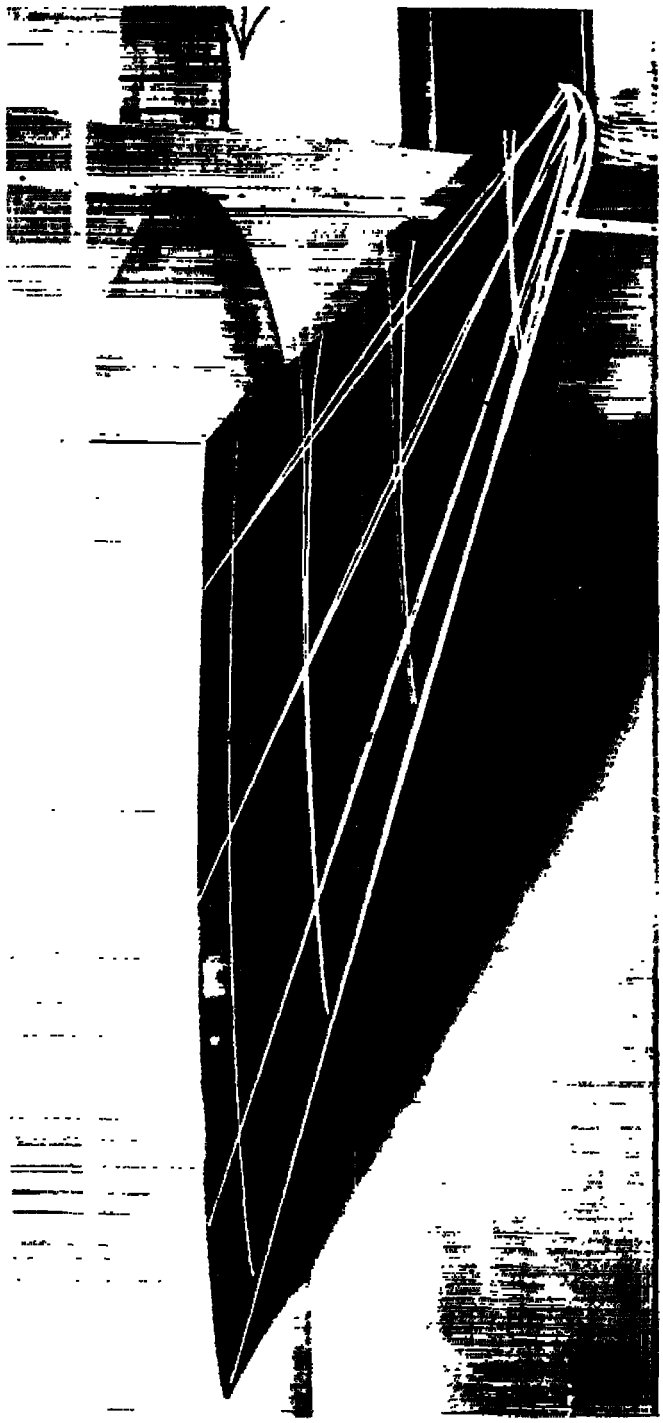

L-95892

(b) Mach number 0.677; frequency, 112.4 cps.

Figure 9.- Continued.

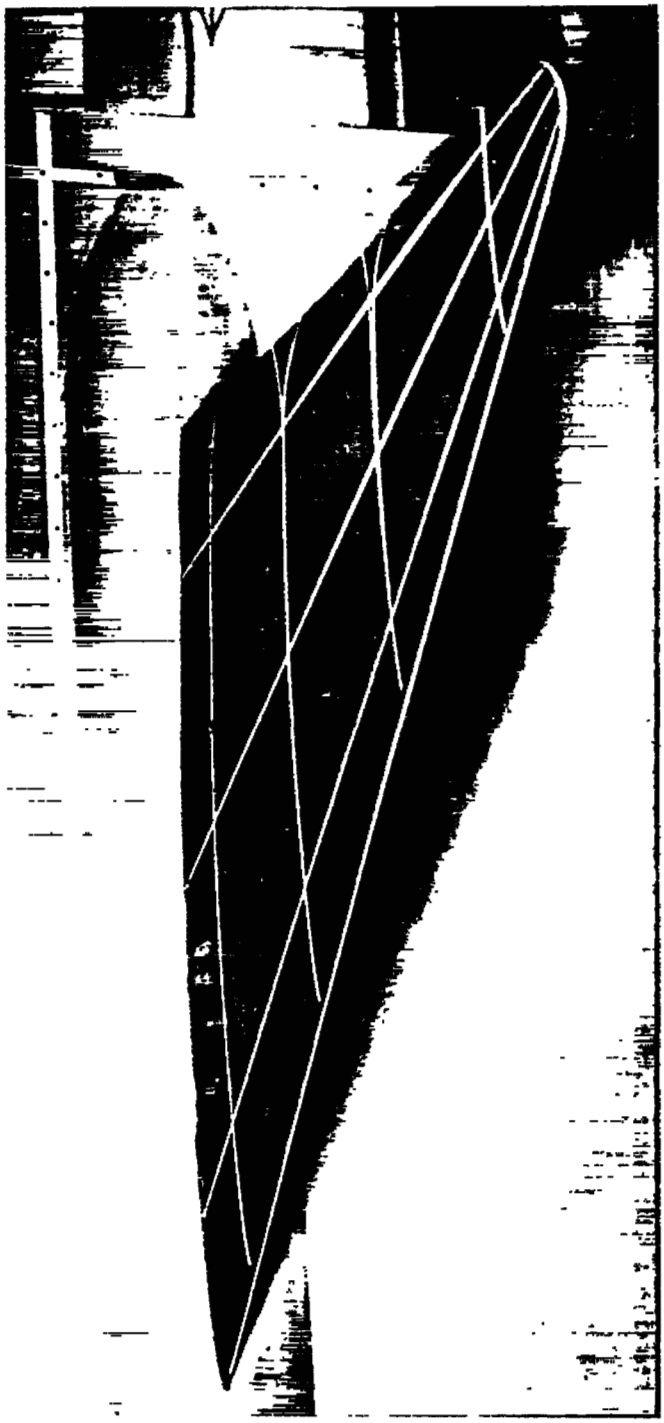

(c) Mach number, 0.808; frequency, 161.8 cps. L-95893

Figure 9.- Continued.

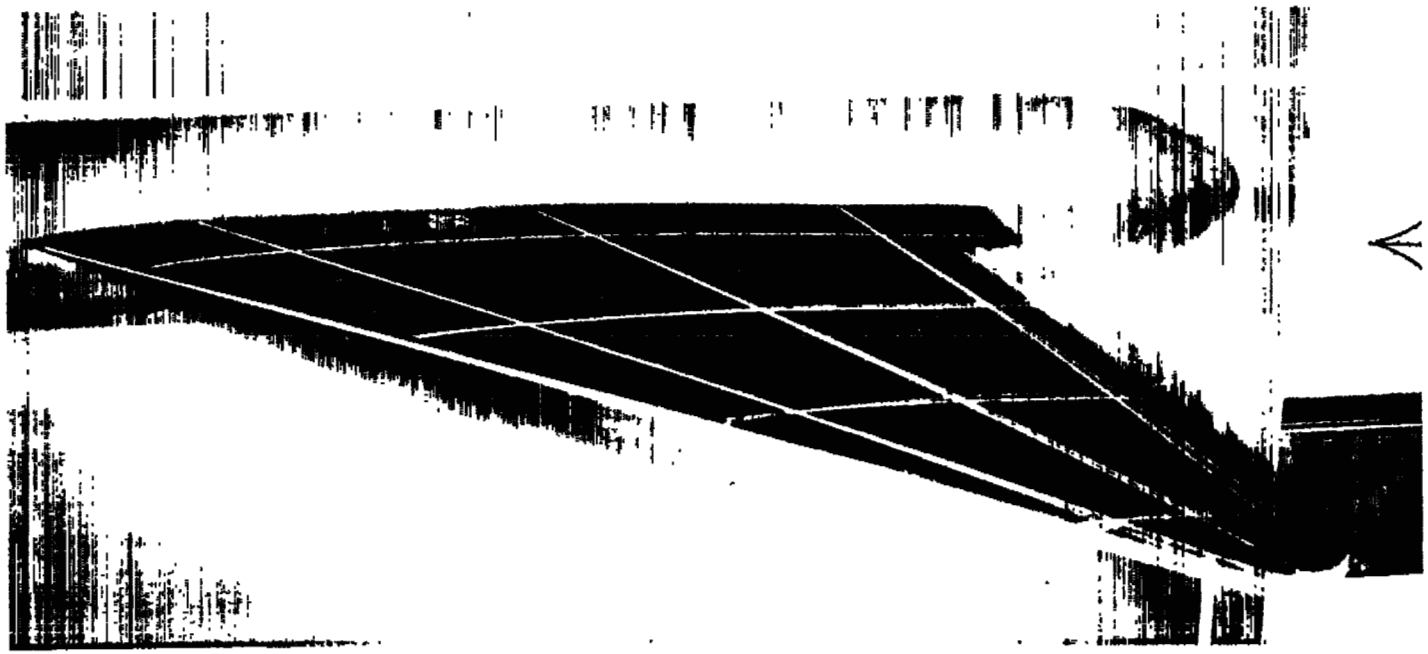

(d) Mach number, 0.669; taken just after failure of trailing edge. L-95894

Figure 9.- Concluded.

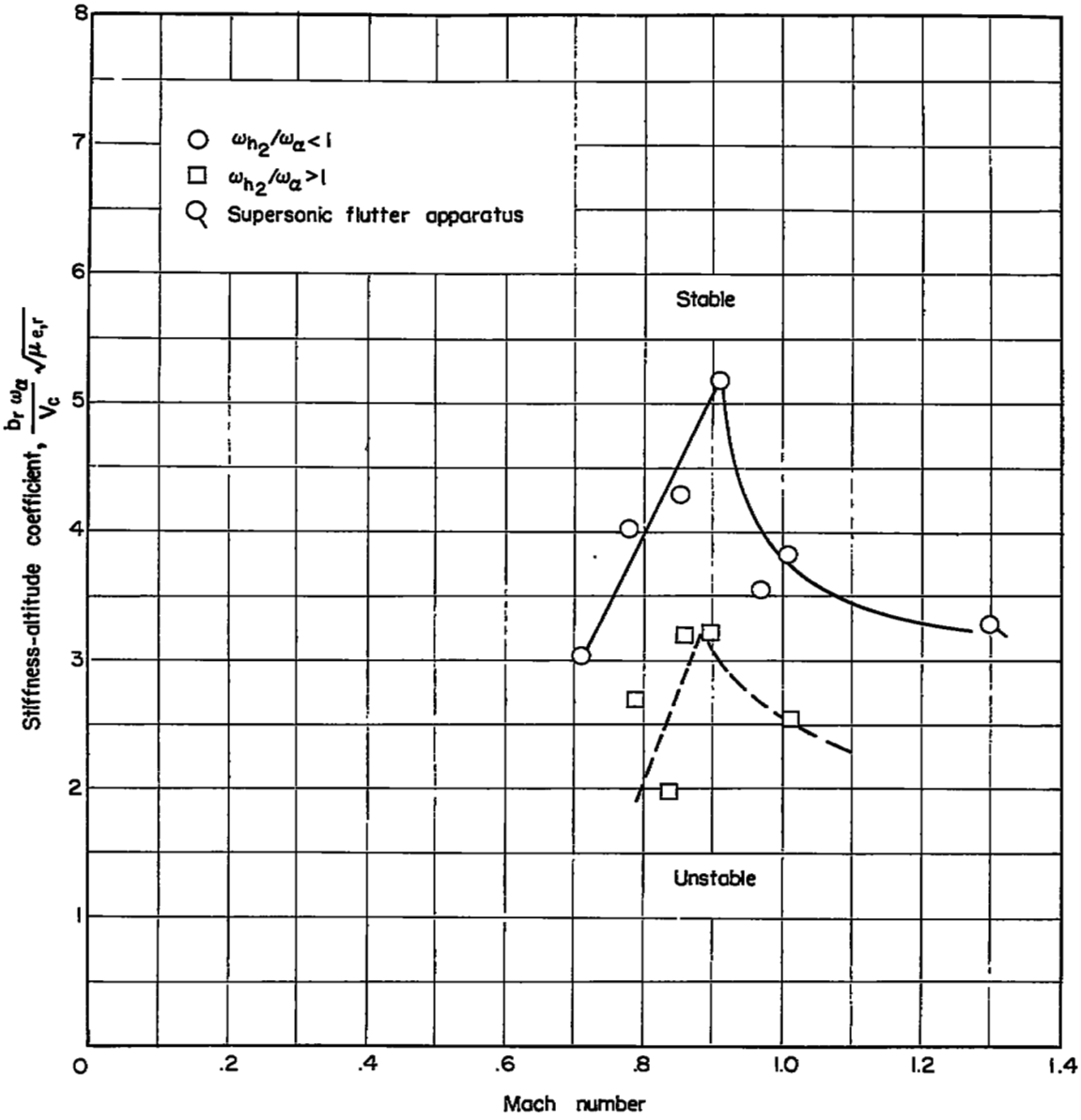

(a) 60° delta wings (except the flat plate).

Figure 10.- Effect of Mach number on the stiffness altitude coefficient, $\frac{b_r \omega_\alpha}{V_c}\sqrt{\mu_{e,r}}$.

[redacted]

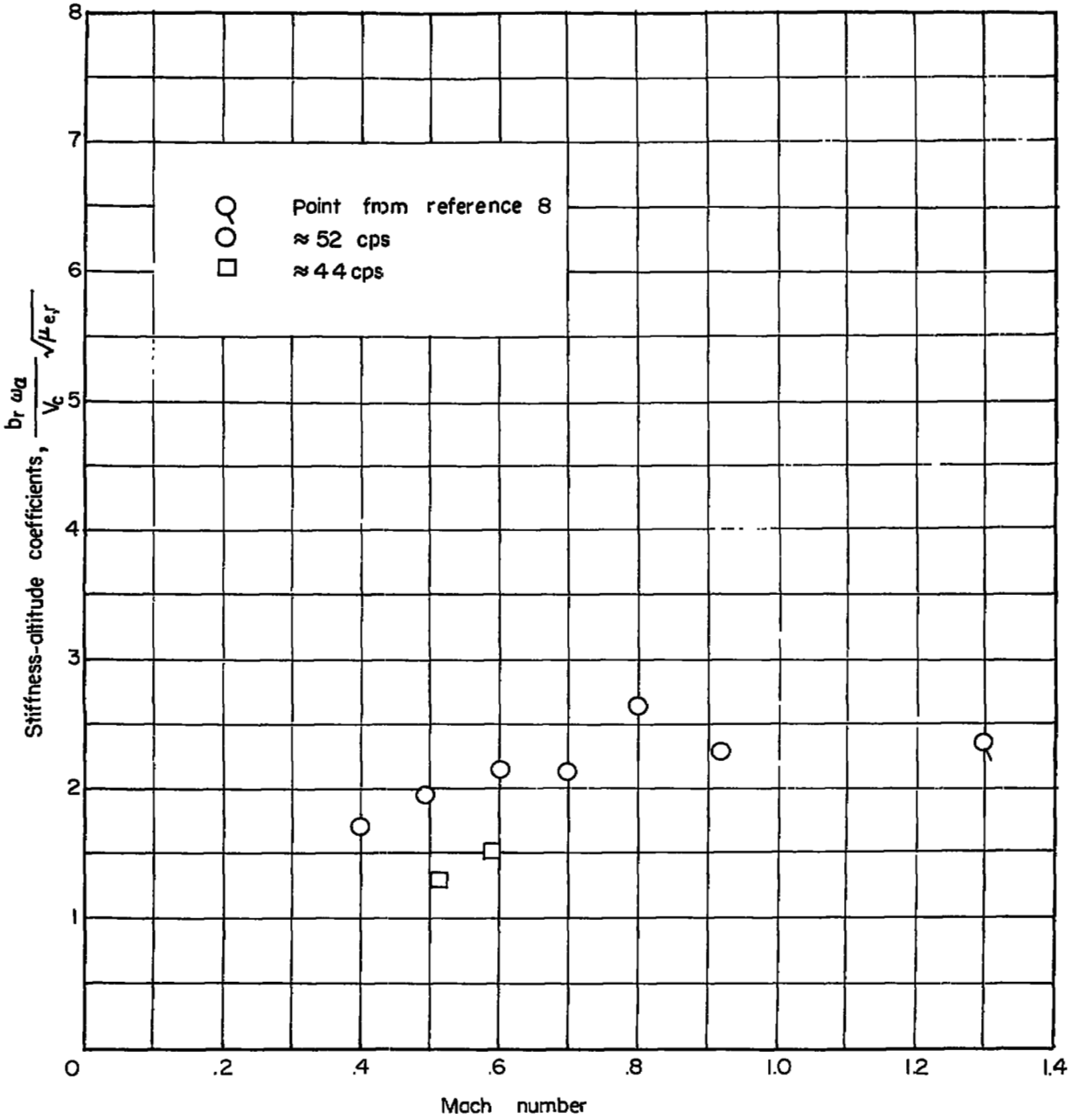

(b) 60° delta flat plate (wing 10).

Figure 10.- Continued.

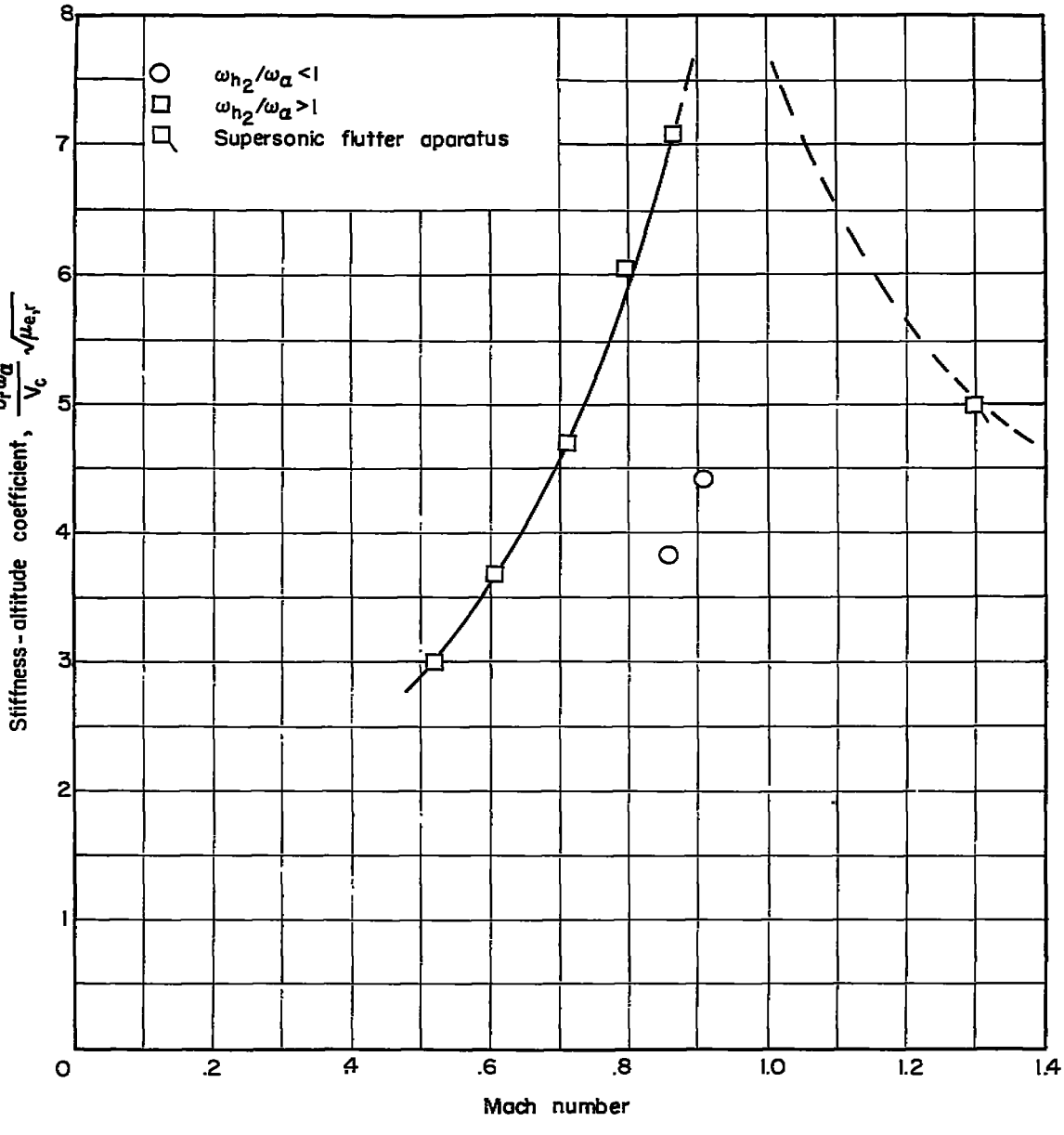

(c) 53° 8' delta wings.

Figure 10.- Concluded.

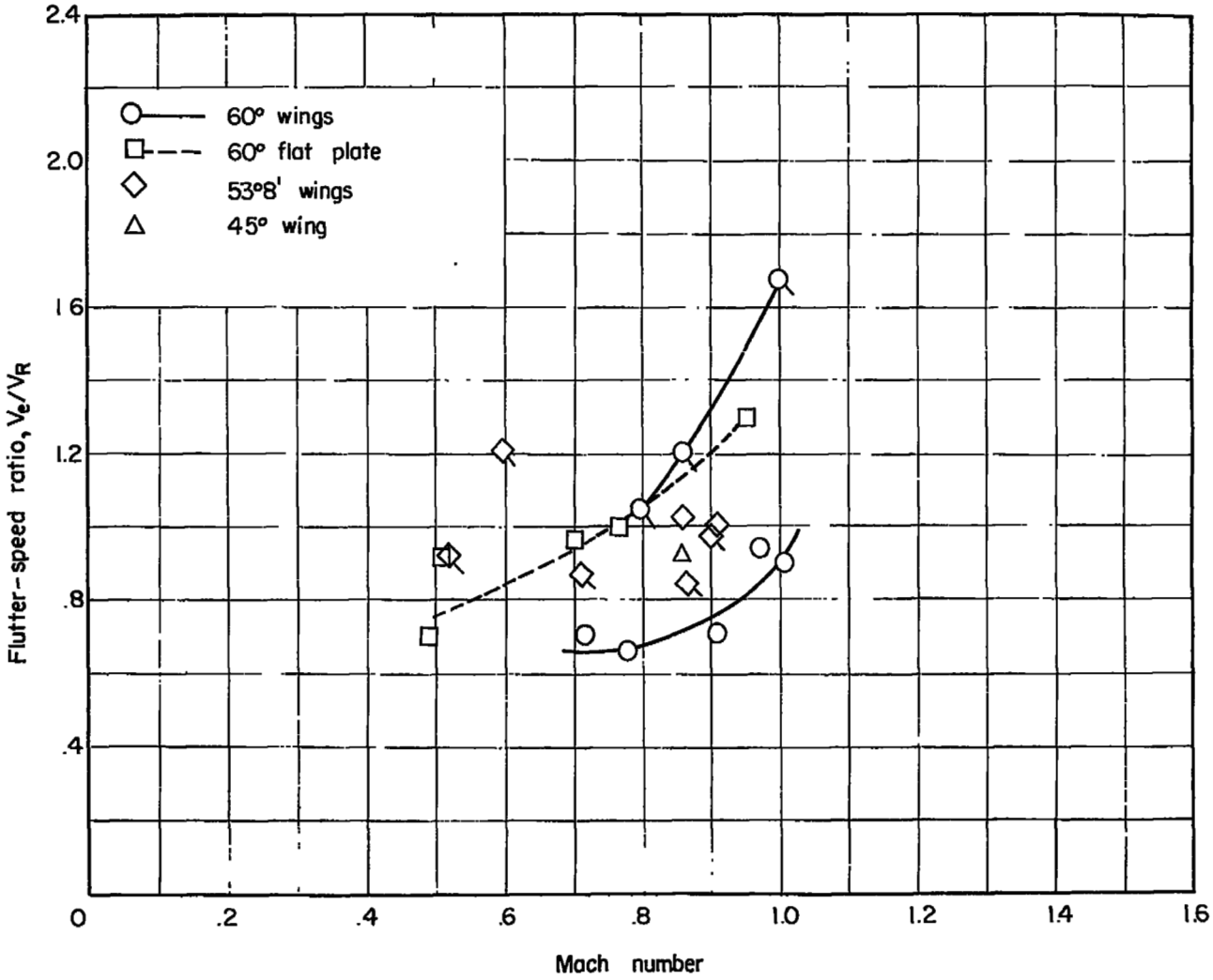

Figure 11.- Plot of flutter speed ratio V_e/V_R against Mach number. Flagged symbols indicate $\omega_{h_2}/\omega_\alpha > 1$.